Biointerface Research in Applied Chemistry
Open-Access Journal (ISSN: 2069-5837)

Article
Volume 13, Issue 5, 2023, 413
https://doi.org/10.33263/BRIAC135.413

Spectral Characterization and Quantum Mechanical Studies of 5-Amino-2-(6-(2-Hydroxyethyl)-3-Oxononyl) Cyclohex-2-Enone Isolated from a Marine Algae

Sheik Rameeza Begum [1], Dasari Jagadeeswara Rao [2,*], Kothagorla Venkata Raghava Rao [3], Yajjala Ramakrishna [4], Natarajan Elangovan [5,6], Thangaiyan Pooventhiran [5,6], Renjith Thomas [5,*]

1 Department of Engineering Physics, S.R.K.R Engineering College, Bhimavaram, A.P, India
2 Department of Physics, SV Degree College, Parvathipuram, Andhra Pradesh, A.P, India
3 Department of Biochemistry, Andhra University, Visakhapatnam, Andhra Pradesh, A.P, India
4 Department of Engineering Physics, A.U College of Engineering, Visakhapatnam, A.P, India
5 Department of Chemistry, St Berchmans College (Autonomous), Mahatma Gandhi University, Changanassery 686101, Kerala, India
6 Department of Mechanical Engineering, University Centre for Research & Development, Chandigarh University, Gharuan, Mohali, Punjab, India
* Correspondence: renjith@sbcollege.ac.in (F.L.); dasarijagadeesh@gmail.com (D.J.R);
Scopus Author ID 55481779800
Received: 7.06.2022; Accepted: 12.10.2022; Published: 22.11.2022

Abstract: The compound C2 was synthesized and characterized with FTIR, FT-Raman, and UV-Vis, compared to experimental and simulated methods. The compound optimized with the DFT method with the WB97D/6311+G(2d,p) basis set level. In FTIR and Raman, the simulated spectrum is in good agreement with the experimental one. The wave function studies like localized orbital locator, electron localized function, average localized ionization energy, and noncovalent interaction were also studied for other theoretical evidence of the titled compound. This compound's ADMET properties are also studied to support the Swiss ADMET online tool. Molecular docking was studied with the help of Autodock/Vina software, with a binding affinity is -7.3 kcal/mol.

Keywords: DFT; IR spectra; NBO; NCI; ALIE.

1. Introduction

Mangroves, saline-resistant ecosystems, are present in tropical and sub-tropical intertidal regions worldwide [1]. Mangrove soil offers a distinct ecological habitat for the growth of diversified microorganisms, which are used in recycling environmental nutrients and producing secondary metabolites of medicinal and industrial importance. Several factors constantly change in the ecosystem, which causes the adaption in metabolic pathways that ultimately leads to the biosynthesis of unique metabolites [2]. The microorganisms residing in the mangrove region include bacteria, fungi, actinomycetes, algae, and fungus-like protozoa. The microbial community of the mangrove ecosystem is 91% bacteria and fungi, 7% of algae, and 2% protozoa. There is extensive microbial biodiversity in this ecosystem; of this, only 1% has been explored, and 99% is not explored [3].

Actinobacteria is aerobic, branched, unicellular gram-positive bacteria with 70% GC content in soil, backwater, lake, and marine environment. It is considered a promising target for screening as it can synthesize novel compounds of therapeutic importance [4].

Actinomycetes, particularly the genus *Streptomyces* is a rich source of secondary metabolites with special attention to antibiotics [5]. Streptomyces possesses numerous high metabolic production rates, recycling in organic matter, and the ability to degrade chitin, lignocelluloses, etc. [6]. These bioactive molecules serve as lead molecules for drug discovery and the development new drugs [7]. Studies were reported on marine actinobacteria, but scanty reports are available concerning actinobacteria from the mangrove ecosystem.

The bioactive compounds produced from streptomycetes include enzymes, pigments, and compounds, which possess antimicrobial, anticancer, antioxidant, immunosuppressive, and other important bioactivities. Particularly antibiotics, whose biosynthesis is connected and are influenced only by primary metabolism but also by the composition of the culture medium. The bioactive compounds are released into the extracellular media, and isolation and purification involve separation techniques, i.e., solvent extraction, chemical precipitation, ion exchange chromatography, HPLC purification, etc. [8]. Further characterization involves mass spectrometry, NMR spectroscopy, and X-ray diffraction [9–13].

50 isolates of actinomycetes were mangrove soil from the area of Visakhapatnam, Andhra Pradesh and named BC 01 - BC 20 and KVR 01 - KVR 30 and maintained on the actinomycetes agar a medium. These isolates are subjected to screening for biological activity [14]. Of these, only four exhibit potent antimicrobial and antioxidant activity. BC_01 exhibits the maximum inhibition of DPPH radical scavenging activity, ferric-reducing antioxidant activity, and total antioxidant activity when compared to others [15]. The morphological, biochemical, and molecular characterization studies reveal that the potent isolate belongs to the genus Streptomyces and the strain's name is *Streptomyces coelicoflavus*. The bioactive fraction was isolated from the fermented broth through column chromatography. Homogeneity and purity of the isolated fractions were determined by TLC and reverse phase HPLC. Further purification procedure was subjected to the separation of three bioactive fractions named BC_C1, BC_C2, and BC_C3. The tentative chemical structure of the fraction was determined by the literature's spectral data and available data. Based on the data the compound was named as 8-(aminomethyl)-7-hydroxy-1-(1-hydroxy-4-(hydroxylmethoxy)-2,3-dimethylbutyl)-2 methyldodecahydro phenanthren-9(1H)-one [16–18].

Computational chemistry tools have emerged as a very good source of information about new compounds [19–21]. This will help people gain detailed information about several experimental materials systems [22–26].

The antibiotic compound C2 8-(aminomethyl)-7-hydroxy-1-(1-hydroxy-4-(hydroxylmethoxy)-2,3-dimethylbutyl)-2-methyldodecahydro phenanthren-9(1H)-one. This compound showed better antimicrobial efficacy against both bacteria and fungi. The minimum inhibitory concentration values for bacteria and fungi are 12.5 - 75 µg/ml and 50 - 125µg/ml, respectively. It exhibits the maximum inhibition of DPPH radical scavenging activity (61.92±6.95), ferric reducing antioxidant activity (56.66±2.51), and total antioxidant activity (67.83±24.79) at a concentration of 20µg/ml. This compound exhibits potent anti-inflammatory activity compared to the standard drug Diclofenac sodium. It also possesses strong *in vitro* cytotoxic potential against various cell lines.

2. Materials and Methods

The compound C2 structure was optimized to the DFT method with WB97D/6311+G(2d,p) basis set method; with the help of the Gaussian software package [27]. The Infrared spectrum was verified from an Agilent spectrometer by KBr pellets, with a range

of 4000- 400 cm-1; FT-Raman was recorded from Bruker RFS-27 Multi RAM FT Raman spectrometer with a range of 4000 – 50 cm^{-1}. Wave function analyses like ELF, LOL, and RDG/noncovalent interaction were calculated with the help of multiwfn software [28][29]. Molecular docking analysis was done by Autodock/Vina software, and protein alignment software using for the discovery studio visualizer.

3. Results and Discussion

3.1. Structural geometry.

The titled compound C2 was optimized with WB97D/6311+G(2d,p) basic set level; [30,31] the optimized structure was shown in Figure 1. The highest bond length, bond angle, and dihedral angle are observed at 1.55, 122.88, and 179.75, corresponding to the C18-H20, C2-C3-O4, and H32-C2-C6-H35, respectively [32,33]. Some bond lengths, bond angles, and dihedral angles are discussed below; C1-C14, C1-H30, C2-H32, C3-C10, C5-H34, C7-C8, C7-H36, C8-H38, C10-H40, C14-C27, C17-H51, C18-H52, C22-H58, C1-C2-C3, C3-C2-H32, C2-C3-C10, H33-C5-H34, C2-C6-H35, C7-C6-H35, C13-C-H39, C8-C11-H48, C11-C12-C16, C15-C14-C27, C14-C15-O28, C12-C14-H50, C18-C17-H51, C20-C18-H52, C14-C1-C2-C3, C14-C1-C2-H32, H31-C1-C2-C6, H30, C1-C14-C15, C6-C2-C3-O4, C1-C2-C6-C7, C3-C2-C6-H35, C2-C3-C10-H41, C15-C5-C6-C2, H39-C9-C10-H49, H44-C12-C16-H50 and C14-C27-N29-H69 corresponding to the 1.53, 1.09, 1.10, 1.51, 1.09, 1.52, .09, .09, 1.08, 1.53, 1.09, 1.09, 1.10, 112.85, 106.14, 114.85, 107.06, 106.33, 106.36, 107.76, 109.68, 109.07, 112.84, 108.74, 112.38, 108.46, 104.79, -179.31, 62.97, -178.17, -66.93, -126.02, -177.37, 64.77, 65.08, -56.40, -177.26, 55.23 and -65.79 respectively [34].

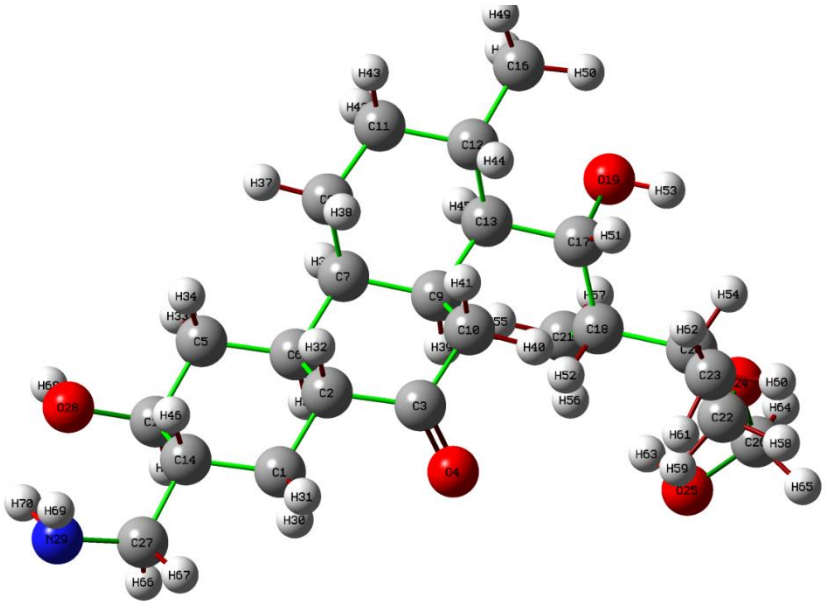

Figure 1. Optimized structure of compound C2.

3.2. Vibrational spectral analysis.

The vibrational spectra of infrared and Raman were recorded using KBr pellets [35,36]. Comparison infrared and Raman spectra are shown in Figure 2 [37]. The NH stretching vibration presented at 3364 cm^{-1} in FT-IR and FT-Raman occurs at 3422 cm^{-1}; normally, NH vibration occurs at 3400-3300 cm^{-1} [38]. In CH, stretching vibration presented at 3014, 2924,

and 2855 cm-1 in infrared and Raman spectra presented at 3214, 3008, and 2921 cm^{-1}. CN stretching vibration was observed at 1653 cm^{-1} in infrared and 1686 cm^{-1} in Raman; [39] the CO stretching vibration was detected at 1246 cm^{-1} in FTIR, and Raman spectra were observed at 1413 cm^{-1}. CH_2 group vibrations are normally observed at six fundamentals: symmetric stretch, asymmetric stretch, scissoring, rocking [40,41], and wagging and twisting vibrations. Asymmetric stretching vibration is generally observed at 3000 cm^{-1}, and symmetric stretching vibration is observed at 3000 to 2900 cm^{-1} [42]. Titled compound CH_2 asymmetric stretching vibration are observed at 3014 cm^{-1} in infrared, Raman asymmetric stretching vibration was observed at 3008 cm^{-1}, and CH_2 symmetric stretching vibrations were noted at 2924 cm^{-1} in FTIR, and FT-Raman is 2921 cm^{-1}. The aromatic CH_2 vibrations of weak to medium can be observed at 1500 to 200 cm^{-1} due to scissoring, wagging, rocking, and twisting vibrations. The above-mentioned vibrations give rise to lower wavenumber and variable intensity bands [43]. In this compound, the band is 1436 and 1410 cm^{-1} for infrared, and Raman is 1413 cm^{-1} in CH_2 scissoring mode [44]. The wagging modes are presented at 1200 to 1000 cm^{-1}, with moderate to strong intensity bonds. The titled compound C2, CH_2 wagging mode is presented at 1023 cm^{-1} in infrared, and CH_2 rocking mode is presented at 1318 cm^{-1}.

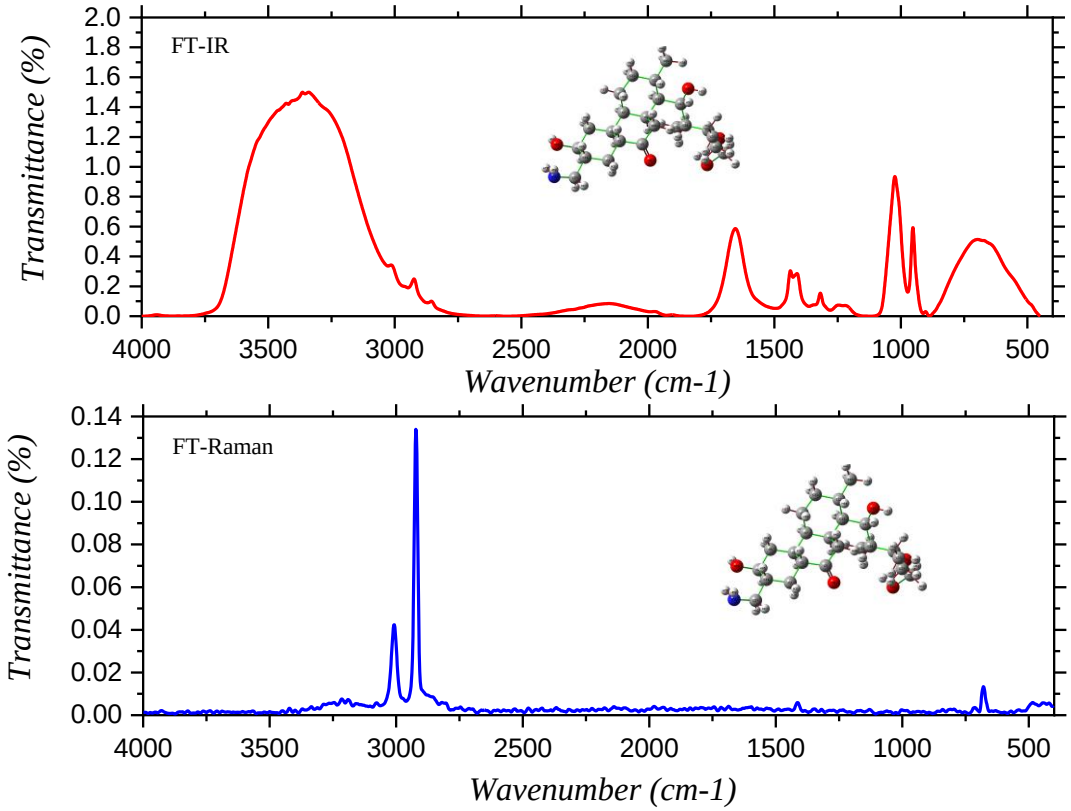

Figure 2. Comparison of Infrared and Raman spectra of the compound C2.

3.3. Molecular electrostatic potential.

The MEP is calculated from the DFT way with WB97D/6311+G(2d,p) basis set [45,46]. Calculate the nucleophilic and electrophilic attack; the molecular electrostatic potential study is very important [47,48]. The blue and red colors are represented more electron-poor and rich regions. MEP surface map is shown in Figure 3; the positive electrostatic potential is located at carbon and all hydrogen atoms, and the negative potential is located at

oxygen and nitrogen atoms [49][50]. Negative and positive electrostatic potentials are clearly indicated by the electrophilic and nucleophilic attack of the compound [51].

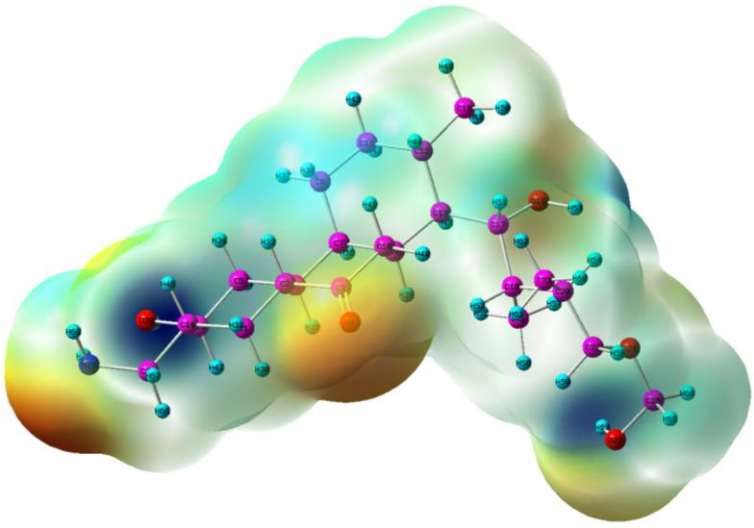

Figure 3. Molecular electrostatic potential surface map of the compound C2.

3.4. Frontier molecular orbital analysis.

Calculating the electrical and chemical properties of the FMO is the most important one [52,53]. The HOMO and LUMO represent the electron donor and acceptor [54]. The HOMO-LUMO energy surface map is shown in fig.4; C2 compound HOMO and LUMO energy are -0.36322eV and 0.18031 eV, with the energy gap, is 5.0 eV [55]. However, the hardness of the titled complex, the HOMO and LUMO energy is higher, and HOMO represents softness and LUMO energy is lower [56]. LUMO is presented at oxygen atoms and carbon atoms; HOMO is presented to an amino group, oxygen atom, and ring [57].

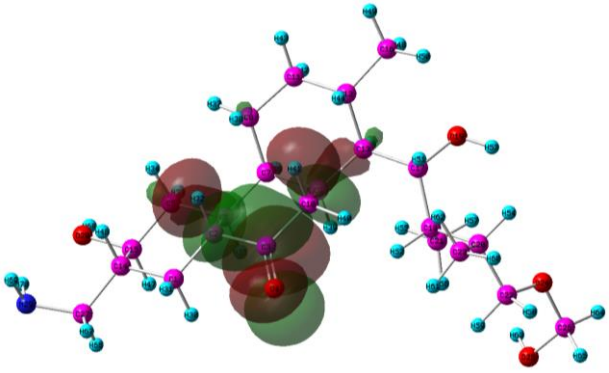

LUMO

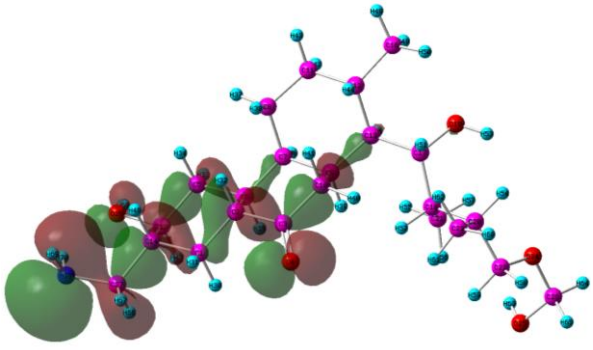

HOMO

Figure 4. HOMO-LUMO surface map of the compound C2.

3.5. Natural population and bond orbital analysis.

The NPA was the distribution of electrons in various subshells; the distribution of electrons is listed in table.S3. The atom N29 has shown the highest electronegativity compared to other electronegative atoms; the value is -0.91534 [58,59]. All carbon atoms have positive and negative charges, and all hydrogen atoms have positive charges; C3 atom showed a highly positive charge compared to other atoms; the charge is 0.57247. In NPA theory, a positive atom accepts electrons and negative atoms donate electrons [60,61].

NBO analysis was determined by intermolecular and intramolecular interactions. C2 complex donor-acceptor interaction was calculated from B3LYP/631G basis set with the help of second-order perturbation theory analysis [62,63]. The donor-acceptor interactions are shown in table.S4 [64,65]. C2 highest stabilization energy is observed at LP(2) O4 to σ*(C2-C3) and σ*(C3-C10), with occupancy is 1.90407 and stabilization energy is 19.03 and 17.98 respectively; and LP(2) O24 to σ*(O25-C26) and LP(2) O25 to σ*(O24-C26), with stabilization energy is 14.75 and 14.04 and occupancy is 1.90770 and 1.93118. Furthermore, the highest stabilization energy noted at σ(C23-H26), σ(C21-H55) to σ*(C18-C20) and σ(C16-H49), σ(C9-H39) to σ*(C12-C13), with stabilization energy is 3.07, 3.62, 3.83 and 3.04 and occupancy is 1.98977, 1.98763, 1.98864 and 1.97318 respectively. The highest stabilization energy observed at σ(C8-H37), σ(C5-H33), and σ(C1-C14) to σ*(C11-C12), σ*(C14-C15) and σ*(C15-O28), with stabilization energy, is 3.38, 3.09 and 3.21 and occupancy is 1.98067, 1.9798 and 1.97123 respectively.

3.6. Topology analysis.

Explain the topology analysis that ELF and LOL are very important [66,67]. The topology analysis is based on the ELF and LOL; the localized orbital locator and localized locator is the maximum electron pair in molecular spacing corresponding to the covalent bond [68]. The electron localized function and localized orbital locators represent the electron pair density due to the orbitals and localized orbital overlapping, respectively [69,70].

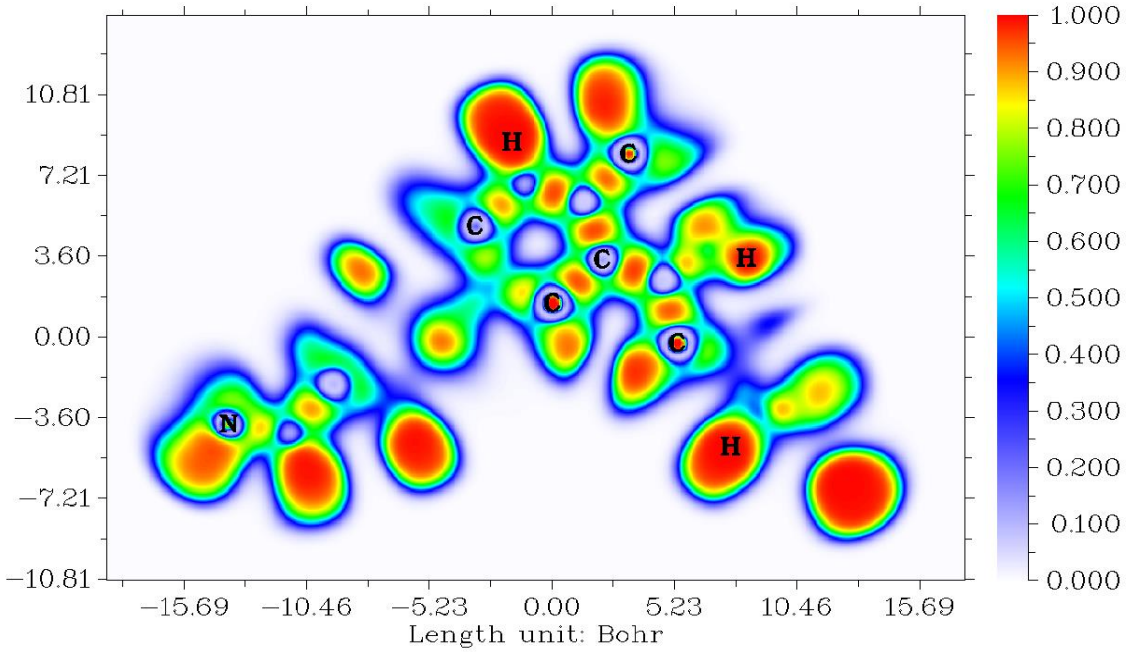

Figure 5. ELF surface map of compound C2.

Analyzing the ELF and LOL, the software used for multiwfn software [28]. The electron localized function and localized orbital locator color coding range is blue to red, and the surface map is shown in Figures 5 and 6. The ELF scale range is 0.000 to 1.000, and the LOL scale range is 0.000 to 0.800; the above color ranges are clearly indicated bonding and non-bonding orbitals [71]. The delocalized electronic region was indicated to be below the 0.5 color range, and the localized electronic region was represented above the 0.5 color range. ELF and LOL surface map, the blue and red represent bonding and non-bonding orbitals [72]. The red and blue colors indicated the maximum electrons of the bonding and non-bonding. The red color was located at hydrogen atoms; the blue color was located at nitrogen and carbon atoms in both ELF and LOL surface maps. The light blue color represents electron reduction on the inner shell and valance; this is located at the oxygen atom and surrounds the whole molecule.

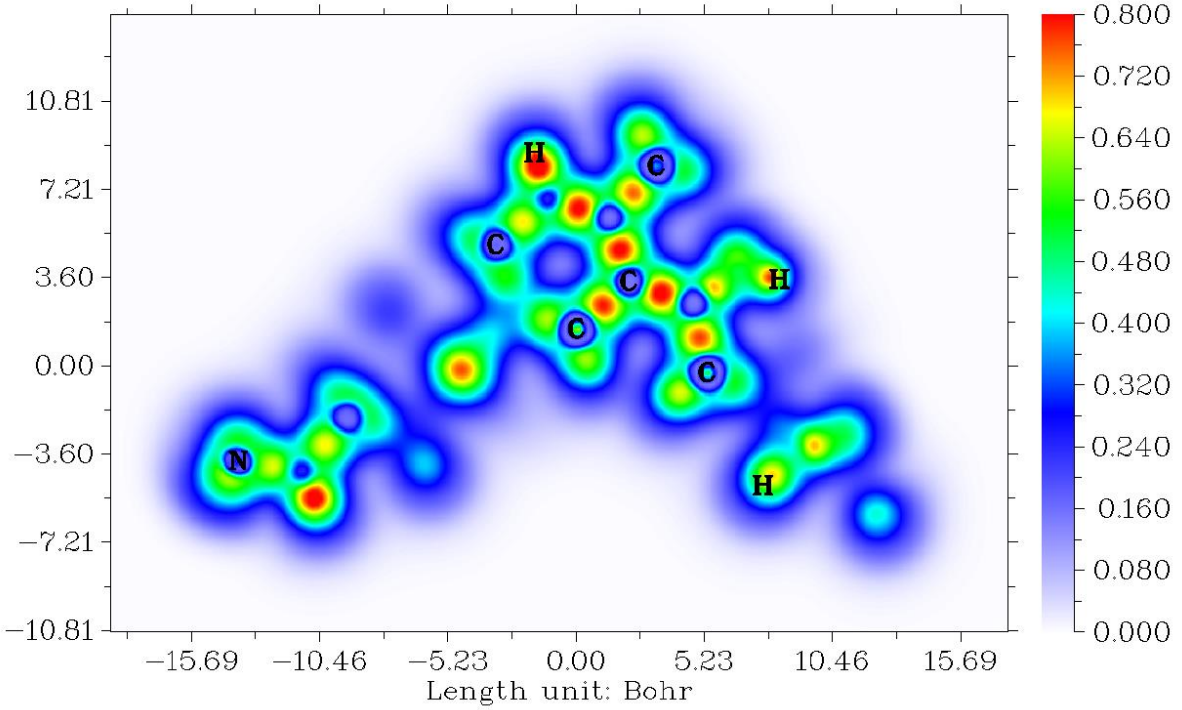

Figure 6. LOL surface map of the compound C2

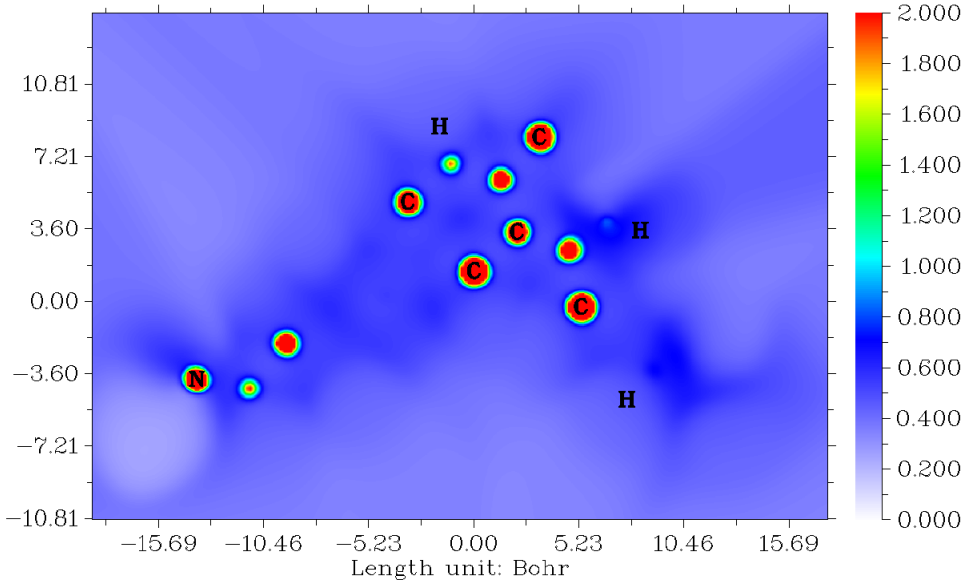

Figure 7. ALIE surface map of compound C2.

3.7. Average localized ionization energy (ALIE).

The average local energy of the compound C2 is needed to remove the electron from the point systems; [73,74] average localized ionization energy is shown in Figure 7. The lowest value of closely held electrons was preferred to the reaction sit of the electrophile or radicals [75,76]. The delocalized electrons indicated a greenish-blue region, greenish blue providing different resonance structures and explaining the stability of the compound; unfortunately, no greenish-blue color was presented [77]. Stable or sigma bond indicated to blue region. Unfortunately, no blue region is presented in this compound. The multiple bonds are denoted at the red region, red color carbon, and nitrogen atoms.

3.8 Non covalent interaction.

RDG was a very useful tool for analyses of the intra- and inter-molecular interactions [73][78]. RDG function was developed by E.R. Johnson *et al.*; the gradient was plotted for RDG vs. electron density, which is shown in Figure 8 [79]. Noncovalent interaction was mainly used to predict the biological activity of the titled compound C2. The above surface map blue color indicates stronger interactive hydrogen bonds, red represents the strongest repulsion, and green represents the Van der Walls interaction of the titled compound [67].

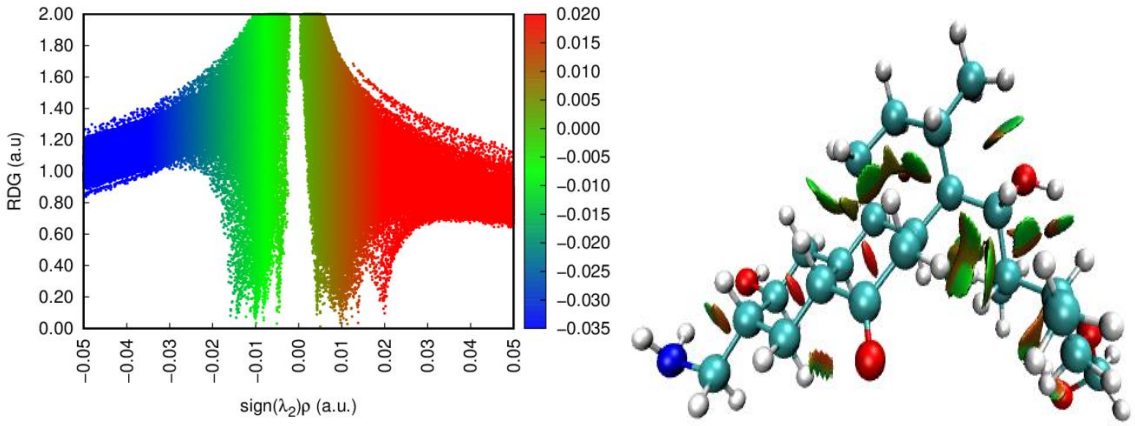

Figure 8. RDG surface map of compound C2.

3.9. Drug likeness.

Drug likeness is called ADME, the ADME was an important technique to calculate the biological property of the titled compound [80]. The Swiss online tool is used for calculating the ADME properties of this compound [81]. Biological property is calculated supporting PASS study results [82]. After the PASS study results, the most important one is the general pump inhibitor, the active probability score is 0.683, and the inactive probability score is 0.009, as listed in Table.1. All physical-chemical properties, namely rotatable bonds, heavy atoms, H-bond donor, H-bond acceptor, bioactivity, TPSA, etc., are given below.

Table 1. PASS study result of the compound C2.

Pa	Pi	Activity
0,683	0,009	General pump inhibitor
0,665	0,029	CYP3A substrate
0,647	0,033	CYP3A4 substrate
0,560	0,046	Proteasome ATPase inhibitor
0,548	0,076	Phosphatase inhibitor
0,501	0,030	Antifungal

Pa	Pi	Activity
0,474	0,019	Antibacterial
0,475	0,025	Antimetastatic
0,392	0,015	Phospholipase A1 inhibitor

3.10. Molecular docking.

Docking studies were done with Autodock/Vina free software package [83]. Earlier protein is downloaded from the RCSB-PDB data bank and prepares the protein by removing water molecules and adding polar hydrogen bonds using Discovery studio visualizer software [84,85]. The protein's active site is definite with 60A0 x 60A0 x 60A0 grid dimension [86]. The compound C2 is docked to the crystal structure of the TetR-like transcription regulator LfrR from *Mycobacterium smegmatis* (2WGB); this is an excellent docking score; [87,88] docking simulation results clearly indicated that the highest docking score is -7.3 kcal/mol and lowest docking score is -6.7 kcal/mol, shown in table.2.

Table 2. The binding affinity of the compound C2.

Mode	Binding Affinity	Distance from msd(l,p)	Best mode msd(u,p)
1	-7.3	0	0
2	-7	4.287	6.637
3	-6.8	13.489	15.255
4	-6.8	5.047	8.6
5	-6.7	2.42	3.46
6	-6.7	3.944	8.736
7	-6.7	13.541	16.054
8	-6.7	3.959	6.84
9	-6.7	25.601	28.105

Table 3. Favorable non-bond interaction of the compound C2.

Distance	Category	Type	From	From-Chem	To	To-Chem
2.81447	HB	Conventional HB	A:ARG148:HH21	H-Donor	:UNK0:O	H-Acceptor
2.72576	HB	Conventional HB	A:ARG148:HH22	H-Donor	:UNK0:O	H-Acceptor
3.05538	HB	Conventional HB	:UNK0:H	H-Donor	B:GLU160:O	H-Acceptor
2.06627	HB	Conventional HB	:UNK0:H	H-Donor	A:ASP125:OD1	H-Acceptor
4.77899	Hydrophobic	Pi-Alkyl	A:TYR107	Pi-Orbitals	:UNK0	Alkyl

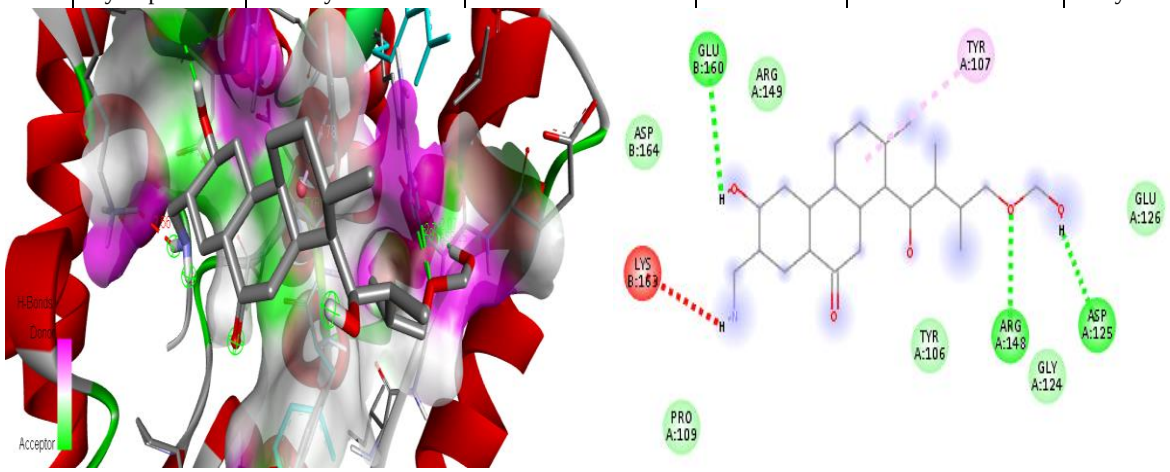

Figure 9. Interaction site of compound C2.

The favorable non-bond interactions are listed in table.5. The compound C2 interacted with protein (2WGB) has shown four conventional hydrogen bonds, namely A:ARG148:HH21 (Arginine), A:ARG148:HH22 (Arginine), B:GLU160:O (Glutamic Acid) and A:ASP125:OD1 (Aspartic Acid) with bond distance is 2.8, 2.7, 3.1 and 2.1 respectively; and one Pi-alkyl bond

such as A:TYR107 (Tyrosine), with bond distance is 4.8. The protein-ligand interaction sites are shown in Figure 9. See Table 3 for details.

4. Conclusions

Compound C2 was synthesized and characterized with a structure like infrared and Raman; after, the compound was compared to theoretical support with the support of Gaussian software. The infrared spectrum experimental and calculated values are closer. This compound is soft because the HOMO-LUMO energy gap is higher; the value is 5.0 eV. Molecular electrostatic potential study of the titled compound is most likely to nucleophile attack. An NPA and natural bond property are also calculated in this study. PASS studies, the active probability score is 0.683; this is the highest score. Drug likeness properties calculated the compound is a biologically active compound. Wave functions were also calculated in this study, namely LOL, ELF, ALIE, and RDG/noncovalent interaction. The molecular simulation studies compound C2 docked to *Mycobacterium smegmatis* (2WGB) protein and confirms the good binding affinity score; the highest binding affinity score is -7.3 kcal/mol.

Funding

RT thanks the Royal Society of Chemistry, London, for support through the Research Fund grant with number R21-6353238377.

Acknowledgments

SEAGrid (http:www.seagrid.org) is acknowledged for computational resources and services for the selected results used in this publication.

Conflicts of Interest

The authors declare no conflict of interest.

References

1. Kemung, H.M.; Tan, L.T.-H.; Chan, K.-G.; Ser, H.-L.; Law, J.W.-F.; Goh, B.H. Streptomyces Sp. Strain MUSC 5 from Mangrove Forest in Malaysia: Identification, Antioxidant Potential and Chemical Profiling of Its Methanolic Extract. *Prog. Microbes Mol. Biol.* **2020**, *3*, https://doi.org/10.36877/pmmb.a0000087.
2. Raghava Rao, K.V.; Mani, P.; Satyanarayana, B.; Raghava Rao, T. Purification and Structural Elucidation of Three Bioactive Compounds Isolated from Streptomyces Coelicoflavus BC 01 and Their Biological Activity. *3 Biotech* **2017**, *7*, https://doi.org/10.1007/s13205-016-0581-9.
3. Xu, J.; Wang, Y.; Xie, S.J.; Xu, J.; Xiao, J.; Ruan, J.S. Streptomyces Xiamenensis Sp. Nov., Isolated from Mangrove Sediment. *Int. J. Syst. Evol. Microbiol.* **2009**, *59*, 472–476, https://doi.org/10.1099/ijs.0.000497-0.
4. Mellouli, L.; Ameur-Mehdi, R. Ben; Sioud, S.; Salem, M.; Bejar, S. Isolation, Purification and Partial Characterization of Antibacterial Activities Produced by a Newly Isolated Streptomyces Sp. US24 Strain. *Res. Microbiol.* **2003**, *154*, 345–352, https://doi.org/10.1016/S0923-2508(03)00077-9.
5. Sharma, S.L.; Pant, A. Crude Oil Degradation by a Marine Actinomycete Rhodococcus Sp. *Indian J. Mar. Sci.* **2001**, *30*, 146–150.
6. Goodfellow, M. Microbial Systematics: Background and Uses. *Appl. Microb. Syst.* **2000**, 1–18, https://doi.org/10.1007/978-94-011-4020-1_1.
7. Chakraborty, I.; Redkar, P.; Munjal, M.; Sathish Kumar, S.R.; Bhaskara Rao, K. V. Isolation and Characterization of Pigment Producing Marine Actinobacteria from Mangrove Soil and Applications of Bio-Pigments. *Der Pharm. Lett.* **2015**, *7*, 93–100, https://www.researchgate.net/profile/Bhaskar-Rao-9/publication/281653426_Isolation_and_characterization_of_pigment_producing_marine_actinobacteria_from_mangrove_soil_and_applications_of_bio-pigments/links/575fe06d08aed884621d8b8d/Isolation-and-characterization-of-pigment-producing-marine-actinobacteria-from-mangrove-soil-and-applications-of-bio-

pigments.pdf.
8. Kim, B.M.; Choi, H.Y.; Kim, G.W.; Zheng, C.J.; Kim, Y.H.; Kim, W.G. Madurahydroxylactone, an Inhibitor of Staphylococcus Aureus FtsZ from Nonomuraea Sp. AN100570. *J. Microbiol. Biotechnol.* **2017**, *27*, 1994–1998, https://doi.org/10.4014/jmb.1708.08044.
9. Irfan, A.; Imran, M.; Thomas, R.; Basra, M.A.R.; Ullah, S.; Al-Sehemi, A.G.; Assiri, M.A. Exploring the Charge Injection Aptitude in Pyrazol and Oxazole Derivatives by the First-Principles Approach. *Zeitschrift für Phys. Chemie* **2022**, *236*, 239–255, https://doi.org/10.1515/zpch-2020-1705.
10. Irfan, A.; Imran, M.; Thomas, R.; Mumtaz, M.W.; Qayyum, M.A.; Ullah, S.; Assiri, M.A.; Al-Sehemi, A.G. Exploration of Electronic Nature and Intrinsic Mobility of 10-(1,3-Dithiol-2-Ylidene)Anthracene Based Organic Semiconductor Materials. *Optik (Stuttg).* **2020**, 165530, https://doi.org/10.1016/j.ijleo.2020.165530.
11. Ramalakshmi, R.; Mary, S.S.; Kirupavathy, S.S.; Muthu, S.; Thomas, R. Growth, Spectral, Optical, Electrical and Computational Analysis of Sodium Oxalate Single Crystals. *Heliyon* **2021**, *7*, e06527, https://doi.org/10.1016/j.heliyon.2021.e06527.
12. Priya, Y.S.; Rao, K.R.; Chalapathi, P. V.; Veeraiah, A.; Srikanth, K.E.; Mary, Y.S.; Thomas, R. Intricate Spectroscopic Profiling, Light Harvesting Studies and Other Quantum Mechanical Properties of 3-Phenyl-5-Isooxazolone Using Experimental and Computational Strategies. *J. Mol. Struct.* **2020**, *1203*, 127461, https://doi.org/10.1016/j.molstruc.2019.127461.
13. Majumdar, D.; Das, S.; Thomas, R.; Ullah, Z.; Sreejith, S.S.; Das, D.; Shukla, P.; Bankura, K.; Mishra, D. Syntheses, X-Ray Crystal Structures of Two New Zn(II)-Dicyanamide Complexes Derived from H2vanen-Type Compartmental Ligands: Investigation of Thermal, Photoluminescence, in Vitro Cytotoxic Effect and DFT-TDDFT Studies. *Inorganica Chim. Acta* **2019**, *492*, 221–234, https://doi.org/10.1016/j.ica.2019.04.041.
14. Hong, K.; Gao, A.H.; Xie, Q.Y.; Gao, H.; Zhuang, L.; Lin, H.P.; Yu, H.P.; Li, J.; Yao, X.S.; Goodfellow, M.; et al. Actinomycetes for Marine Drug Discovery Isolated from Mangrove Soils and Plants in China. *Mar. Drugs* **2009**, *7*, 24–44, https://doi.org/10.3390/md7010024.
15. Raghava Rao, K.V.; Raghava Rao, T. Molecular Characterization and Its Antioxidant Activity of a Newly Isolated Streptomyces Coelicoflavus BC 01 from Mangrove Soil. *J. Young Pharm.* **2013**, *5*, 121–126, https://doi.org/10.1016/j.jyp.2013.10.002.
16. Al-zaqri, N.; Pooventhiran, T.; Alsalme, A.; Warad, I.; John, A.M.; Thomas, R. Structural and Physico-Chemical Evaluation of Melatonin and Its Solution-State Excited Properties, with Emphasis on Its Binding with Novel Coronavirus Proteins. *J. Mol. Liq.* **2020**, *318*, 114082, https://doi.org/10.1016/j.molliq.2020.114082.
17. John, A.M.; Thomas, R.; Balakrishnan, S.P.; Al-Zaqri, N.; Alsalme, A.; Warad, I. Diazo-Pyrazole Analogues as Photosensitizers in Dye Sensitised Solar Cells: Tuning for a Better Photovoltaic Efficiency Using a New Modelling Strategy Using Experimental and Computational Data. *Zeitschrift für Phys. Chemie* **2021**, https://doi.org/10.1515/ZPCH-2020-1722.
18. John, A.M.; Jose, J.; Thomas, R.; Thomas, K.J.; Balakrishnan, S.P. Spectroscopic and TDDFT Investigation of Highly Selective Fluoride Sensors by Substituted Acyl Hydrazones. *Spectrochim. Acta Part A Mol. Biomol. Spectrosc.* **2020**, 118329, https://doi.org/10.1016/j.saa.2020.118329.
19. Agwupuye, J.A.; Louis, H.; Unimuke, T.O.; David, P.; Ubana, E.I.; Moshood, Y.L. Electronic Structure Investigation of the Stability, Reactivity, NBO Analysis, Thermodynamics, and the Nature of the Interactions in Methyl-Substituted Imidazolium-Based Ionic Liquids. *J. Mol. Liq.* **2021**, *337*, 116458, https://doi.org/10.1016/j.molliq.2021.116458.
20. Louis, H.; Gber, T.E.; Asogwa, F.C.; Eno, E.A.; Unimuke, T.O.; Bassey, V.M.; Ita, B.I. Understanding the Lithiation Mechanisms of Pyrenetetrone-Based Carbonyl Compound as Cathode Material for Lithium-Ion Battery: Insight from First Principle Density Functional Theory. *Mater. Chem. Phys.* **2022**, *278*, 125518, https://doi.org/10.1016/j.matchemphys.2021.125518.
21. Bisong, E.A.; Louis, H.; Unimuke, T.O.; Odey, J.O.; Ubana, E.I.; Edim, M.M.; Tizhe, F.T.; Agwupuye, J.A.; Utsu, P.M. Vibrational, Electronic, Spectroscopic Properties, and NBO Analysis of p-Xylene, 3,6-Difluoro-p-Xylene, 3,6-Dichloro-p-Xylene and 3,6-Dibromo-Pxylene: DFT Study. *Heliyon* **2020**, *6*, e05783, https://doi.org/10.1016/j.heliyon.2020.e05783.
22. Ferin Fathima, A.; Jothi Mani, R.; Sakthipandi, K.; Manimala, K.; Hossain, A. Enhanced Antifungal Activity of Pure and Iron-Doped ZnO Nanoparticles Prepared in the Absence of Reducing Agents. *J. Inorg. Organomet. Polym. Mater.* **2020**, *30*, 2397–2405, https://doi.org/10.1007/s10904-019-01400-z.
23. Ahilandeswari, E.; Sakthipandi, K.; Rajesh Kanna, R.; Hubálovská, M.; Vigneswaran, D. Lanthanum Substitution Effect on the Structural, Optical, and Dielectrical Properties of Nanocrystalline BaFe2O4 Ferrites. *Phys. B Condens. Matter* **2022**, *635*, 413849, https://doi.org/10.1016/j.physb.2022.413849.
24. Sankarrajan, S.; Sakthipandi, K.; Manivasakan, P.; Thyagarajan, K.; Rajendran, V. On-Line Phase Transition in La1− x Sr x MnO3 ($0.28 \leq x \leq 0.36$) Perovskites through Ultrasonic Studies. *Phase Transitions* **2011**, *84*, 657–672, https://doi.org/10.1080/01411594.2011.556915.
25. Ahilandeswari, E.; Rajesh Kanna, R.; Sakthipandi, K. Synthesis of Neodymium-Doped Barium Nanoferrite: Analysis of Structural, Optical, Morphological, and Magnetic Properties. *Phys. B Condens. Matter* **2020**, *599*, 412425, https://doi.org/10.1016/j.physb.2020.412425.
26. Sakthipandi, K.; Rajendran, V. On-Line Phase Transitions of Bulk and Nanocrystalline La1−xPbxMnO3

(X=0.3, 0.4, and 0.5) Perovskite Manganite Materials Using Ultrasonic Measurements. *Mater. Chem. Phys.* **2013**, *138*, 581–592, https://doi.org/10.1016/j.matchemphys.2012.12.023.
27. Frisch, M.J.; Trucks, G.W.; Schlegel, H.B.; Scuseria, G.E.; Robb, M.A.; Cheeseman, J.R.; Scalmani, G.; Barone, V.; Mennucci, B.; Petersson, G.A.; et al. Gaussian 09, Revision B.01. *Gaussian 09, Revis. B.01, Gaussian, Inc., Wallingford CT* **2009**, 1–20,
28. Lu, T.; Chen, F. Multiwfn: A Multifunctional Wavefunction Analyzer. *J. Comput. Chem.* **2012**, *33*, 580–592, https://doi.org/10.1002/jcc.22885.
29. Tsirelson, V.; Stash, A. Determination of the Electron Localization Function from Electron Density. *Chem. Phys. Lett.* **2002**, *351*, 142–148, https://doi.org/10.1016/S0009-2614(01)01361-6.
30. Bouchoucha, A.; Zaater, S.; Bouacida, S.; Merazig, H.; Djabbar, S. Synthesis and Characterization of New Complexes of Nickel (II), Palladium (II) and Platinum(II) with Derived Sulfonamide Ligand: Structure, DFT Study, Antibacterial and Cytotoxicity Activities. *J. Mol. Struct.* **2018**, https://doi.org/10.1016/j.molstruc.2018.02.057.
31. Hamad, A.; Khan, M.A.; Rahman, K.M.; Ahmad, I.; Ul-haq, Z.; Khan, S.; Shafiq, Z. Development of Sulfonamide-Based Schiff Bases Targeting Urease Inhibition : Synthesis, Characterization, Inhibitory Activity Assessment, Molecular Docking and ADME Studies . *Bioorg. Chem.* **2020**, 104057, https://doi.org/10.1016/j.bioorg.2020.104057.
32. Arunachalam, M.; Thamilmaran, P.; Sakthipandi, K. Tunning of Metal-Insulator Phase Transition Temperature in La0.3Ca0.7MnO3 Perovskite Material. *Mater. Lett.* **2018**, *218*, 270–273, https://doi.org/10.1016/j.matlet.2018.02.032.
33. Senthilkumar, G.S.; Sankarganesh, M.; Dhaveethu Raja, J.; Adwin Jose, P.R.; Sakthivel, A.; Christopher Jeyakumar, T.; Nandini Asha, R. Water Soluble Cu(II) and Zn(II) Complexes of Bidentate-Morpholine Based Ligand: Synthesis, Spectral, DFT Calculation, Biological Activities and Molecular Docking Studies. *J. Biomol. Struct. Dyn.* **2022**, *40*, 1074–1083, https://doi.org/10.1080/07391102.2020.1821783.
34. Quintana, C.; Silva, G.; Klahn, A.H.; Artigas, V.; Fuentealba, M.; Biot, C.; Halloum, I.; Kremer, L.; Novoa, N.; Arancibia, R. New Cyrhetrenyl and Ferrocenyl Sulfonamides: Synthesis, Characterization, X-Ray Crystallography, Theoretical Study and Anti-Mycobacterium Tuberculosis Activity. *Polyhedron* **2017**, *134*, 166–172, https://doi.org/10.1016/j.poly.2017.06.015.
35. Kumar, V.S.; Mary, Y.S.; Pradhan, K.; Brahman, D.; Mary, Y.S.; Thomas, R.; Roxy, M.S.; Alsenoy, C. Van Synthesis, Spectral Properties, Chemical Descriptors and Light Harvesting Studies of a New Bioactive Azo Imidazole Compound. *J. Mol. Struct.* **2020**, *1199*, 127035, https://doi.org/10.1016/j.molstruc.2019.127035.
36. Karpagakalyaani, G.; Magdaline, J.D.; Chithambarathanu, T.; Aruldhas, D.; Anuf, A.R. Spectroscopic (FT-IR, FT-Raman, NBO) Investigation and Molecular Docking Study of a Herbicide Compound Bifenox. **2020**, *27*, https://doi.org/10.1016/j.cdc.2020.100393.
37. Venil, K.; Lakshmi, A.; Balachandran, V.; Narayana, B.; Salian, V. V FT-IR and FT-Raman Investigation, Quantum Chemical Analysis and Molecular Docking Studies Of. *J. Mol. Struct.* **2021**, *1225*, 129070, https://doi.org/10.1016/j.molstruc.2020.129070.
38. Thamilmaran, P.; Arunachalam, M.; Sankarrajan, S.; Sakthipandi, K. On-Line Ultrasonic Characterisation of Barium Doped Lanthanum Perovskites. *Phys. B Condens. Matter* **2015**, *466–467*, 19–25, https://doi.org/10.1016/j.physb.2015.03.017.
39. Manjusha, P.; Christian, J.; Muthu, S.; Rizwana, B.F. Spectroscopic Elucidation (FT-IR, FT-Raman and UV-Visible) with NBO, NLO, ELF, LOL, Drug Likeness and Molecular Docking Analysis on 1- (2-Ethylsulfonylethyl) -2-Methyl-5-Nitro-Imidazole : An Antiprotozoal Agent. *Comput. Biol. Chem.* **2020**, *88*, 107330, https://doi.org/10.1016/j.compbiolchem.2020.107330.
40. Brizuela, A.B.; Raschi, A.B.; Castillo, M. V; Davies, L.; Brandán, S.A. Structural and Vibrational Investigation on Species Derived from the Cyclamic Acid in Aqueous Solution by Using HATR and Raman Spectroscopies and SCRF Calculations. *J. Mol. Struct.* **2014**, https://doi.org/10.1016/j.molstruc.2014.05.019.
41. Alphonsa, A.T.; Loganathan, C.; Athavan, S.; Kabilan, S. AC SC. *J. Mol. Struct.* **2015**, https://doi.org/10.1016/j.molstruc.2015.07.024.
42. Paularokiadoss, F.; Christopher Jeyakumar, T.; Thomas, R.; Sekar, A.; Bhakiaraj, D. Group 13 Monohalides [AX (A = B, Al, Ga and In; X = Halogens)] as Alternative Ligands for Carbonyl in Organometallics: Electronic Structure and Bonding Analysis. *Comput. Theor. Chem.* **2022**, *1209*, 113587, https://doi.org/10.1016/j.comptc.2021.113587.
43. Sevvanthi, S.; Muthu, S.; Aayisha, S.; Ramesh, P.; Raja, M. Spectroscopic (FT-IR, FT-Raman and UV-Vis), Computational (ELF, LOL, NBO, HOMO-LUMO, Fukui, MEP) Studies and Molecular Docking on Benzodiazepine Derivatives- Heterocyclic Organic Arenes. *Chem. Data Collect.* **2020**, *30*, 100574, https://doi.org/10.1016/j.cdc.2020.100574.
44. Chandralekha, B.; Hemamalini, R.; Muthu, S.; Sevvanthi, S. Spectroscopic (FT-IR, FT-RAMAN, NMR, UV e Vis) Investigations, Computational Analysis and Molecular Docking Study of 5-Bromo-2- Hydroxy Pyrimidine. *J. Mol. Struct.* **2020**, *1218*, 128494, https://doi.org/10.1016/j.molstruc.2020.128494.
45. Sarojini, K.; Krishnan, H.; Kanakam, C.C.; Muthu, S. Spectrochimica Acta Part A : Molecular and Biomolecular Spectroscopy Synthesis, X-Ray Structural, Characterization, NBO and HOMO – LUMO Analysis Using DFT Study of 4-Methyl- N - (Naphthalene-1-Yl) Benzene Sulfonamide. *Spectrochim. ACTA*

PART A Mol. Biomol. Spectrosc. **2012**, *96*, 657–667, https://doi.org/10.1016/j.saa.2012.07.037.
46. Charge-Transfer Complexes of Hypoglycemic Sulfonamide with π-Acceptors. *J. Mol. Struct.* **2019**, *1175,105-116*, https://doi.org/10.1016/j.molstruc.2018.07.074.
47. Elangovan, N.; Sowrirajan, S. Heliyon Synthesis, Single Crystal (XRD), Hirshfeld Surface Analysis, Computational Study (DFT) and Molecular Docking Studies of (E) -4- ((2-Hydroxy-3, 5-Diio. *Heliyon* **2021**, *7*, e07724, https://doi.org/10.1016/j.heliyon.2021.e07724.
48. Elangovan, N.; Gangadharappa, B.; Thomas, R.; Irfan, A. Synthesis of a Versatile Schiff Base 4-((2-Hydroxy-3,5-Diiodobenzylidene) Amino) Benzenesulfonamide from 3,5-Diiodosalicylaldehyde and Sulfanilamide, Structure, Electronic Properties, Biological Activity Prediction and Experimental Antimicrobial Propertie. *J. Mol. Struct.* **2021**, 131700, https://doi.org/10.1016/j.molstruc.2021.131700.
49. Elangovan, N.; Thomas, R.; Sowrirajan, S.; Irfan, A. Journal of the Indian Chemical Society Synthesis, Spectral and Quantum Mechanical Studies and Molecular Docking Studies of Schiff Base (E) 2-Hydroxy-5- (((4- (N-Pyrimidin-2-Yl) Sulfamoyl) Phenyl) Imino) Methyl Benzoic Acid from 5-Formyl Salicylic. *J. Indian Chem. Soc.* **2021**, *98*, 100144, https://doi.org/10.1016/j.jics.2021.100144.
50. Innasiraj, A.; Andhi, B.; Gnanadeepam, Y.; Das, N.; Paularokiadoss, F.; Ilavarasi, A.V.; Sheela, C.D.; Ampasala, D.R.; Jeyakumar, T.C. Experimental and Theoretical Studies of Novel Schiff Base Based on Diammino Benzophenone with Formyl Chromone - BPAMC. *J. Mol. Struct.* **2022**, *1265*, 133450, https://doi.org/10.1016/j.molstruc.2022.133450.
51. Anaikutti, P.; Selvaraj, M.; Prabhakaran, J.; Pooventhiran, T.; Jeyakumar, T.C.; Thomas, R.; Makam, P. Indolyl-4H-Chromenes: Multicomponent One-Pot Green Synthesis, in Vitro and in Silico, Anticancer and Antioxidant Studies. *J. Mol. Struct.* **2022**, *1266*, 133464, https://doi.org/10.1016/j.molstruc.2022.133464.
52. Elangovan, N.; Thomas, R.; Sowrirajan, S.; Manoj, K.P.; Irfan, A.; Thomas, R.; Sowrirajan, S.; Manoj, K.P.; Irfan, A. Synthesis, Spectral Characterization, Electronic Structure and Biological Activity Screening of the Schiff Base 4- ((4-Hydroxy-3-Methoxy-5- Yl) Benzene Sulfonamide from 5-Nitrovaniline and Sulphadiazene. *Polycycl. Aromat. Compd.* **2021**, *0*, 1–18, https://doi.org/10.1080/10406638.2021.1991392.
53. Arshad, M.N.; Hussain, M.M.; Asiri, A.M.; Khalid, M.; Braga, A.A.C.; Rahman, M.M. A Potent Synthesis and Supramolecular Synthon Hierarchy Percipience of (E)-N′-(Napthalen-1-Yl-Methylene)-Benzenesulfonohydrazide and 1-Napthaldehyde: A Combined Experimental and DFT Studies. *J. Mol. Struct.* **2020**, *1221*, 128797, https://doi.org/10.1016/j.molstruc.2020.128797.
54. Mondal, S.; Mandal, S.M.; Mondal, T.K.; Sinha, C. Spectroscopic Characterization, Antimicrobial Activity, DFT Computation and Docking Studies of Sulfonamide Schiff Bases. *J. Mol. Struct.* **2016**, https://doi.org/10.1016/j.molstruc.2016.08.011.
55. Pahuja, A.; Jeyakumar, T.C.; Paularokiadoss, F. Structural Analysis and Chemical Descriptors Analysis of 4-Aminopyridine Adsorbed on M4 (M = Co, Ni, Cu) Clusters: A DFT Study. *Vietnam J. Chem.* **2022**, *60*, 376–388, https://doi.org/10.1002/vjch.202100150.
56. Ge, P.; Yu, H.; Chen, J.; Qu, J.; Luo, Y. Photolysis Mechanism of Sulfonamide Moiety in Five-Membered Sulfonamides: A DFT Study. *Chemosphere* **2018**, *197*, 569–575, https://doi.org/10.1016/j.chemosphere.2018.01.041.
57. Karrouchi, K.; Brandán, S.A.; Sert, Y.; El-marzouqi, H.; Radi, S.; Ferbinteanu, M.; El, M.; Faouzi, A.; Garcia, Y.; Ansar, M. Synthesis, X-Ray Structure, Vibrational Spectroscopy, DFT, Biological Evaluation and Molecular Docking Studies of (E)-N'-(4-(Dimethylamino)Benzylidene)-5-Methyl-1H-Pyrazole-3-Carbohydrazide. *J. Mol. Struct.* **2020**, 128541, https://doi.org/10.1016/j.molstruc.2020.128541.
58. Ft-ir, T.; Function, F. NPA and Tautomerism Effect Analysis of (E) -2- [(2-Hydroxy-6-Methoxybenzylidene) Amino] Benzonitrile. *Spectrochim. ACTA PART A Mol. Biomol. Spectrosc.* **2014**, https://doi.org/10.1016/j.saa.2014.11.078.
59. Frank, A.K.; Demircio, Z. Spectroscopic, XRD, Hirshfeld Surface and DFT Approach (Chemical Activity, ECT, NBO, FFA, NLO, MEP, NPA & MPA) of (E) -4-Bromo-2- [(4- Bromophenylimino) Methyl] -6-Ethoxyphenol Zeynep Demircio G. **2019**, *1191*, https://doi.org/10.1016/j.molstruc.2019.03.060.
60. Velraj, G.; Soundharam, S.; Sridevi, C. Structure, Vibrational, Electronic, NBO and NMR Analyses of 3-Methyl-2, 6-Diphenylpiperidin-4-One (MDPO) by Experimental and Theoretical Approach. *J. Mol. Struct.* **2014**, *1060*, 156–165, https://doi.org/10.1016/j.molstruc.2013.12.040.
61. Durgun, M.; Turkmen, H.; Turkmen, H. AC SC. **2016**, *1114*, 95-107, https://doi.org/10.1016/j.molstruc.2016.02.062.
62. Ceylan, Ü.; Durgun, M.; Türkmen, H. Theoretical and Experimental Investigation of 4- [(2-Hydroxy-3-Methylbenzylidene) Amino] Benzenesulfonamide : Structural and Spectroscopic Properties, NBO, NLO and NPA Analysis. **2015**, *1089*, 222–232, https://doi.org/10.1016/j.molstruc.2015.02.042.
63. Mumit, M.A.; Pal, T.K.; Alam, A.; Islam, A.; Paul, S.; Sheikh, C. DFT Studies on Vibrational and Electronic Spectra, HOMO–LUMO, MEP, HOMA, NBO and Molecular Docking Analysis of Benzyl-3-N-(2,4,5-Trimethoxyphenylmethylene)Hydrazinecarbodithioate. *J. Mol. Struct.* **2020**, 128715, https://doi.org/10.1016/j.molstruc.2020.128715.
64. Amin, M.; Haddad, B.; Antonia, S.; Paolone, A.; Villemin, D.; Bresson, S. Bidentate Cation-Anion Coordination in the Ionic Liquid 1-Ethyl-3- Methylimidazolium Hexa Fl Uorophosphate Supported by Vibrational Spectra and NBO, AIM and SQMFF Calculations. **2020**, *1212*, 1–14,

https://doi.org/10.1016/j.molstruc.2020.128104.
65. Anal-, N.B.O. Structural, Spectral, Thermodynamical, NLO, HOMO, LUMO and NBO Analysis of Fluconazole. *Spectrochim. ACTA PART A Mol. Biomol. Spectrosc.* **2015**, *150*, 974-991, https://doi.org/10.1016/j.saa.2015.06.018.
66. Lu, T.; Chen, Q. Van Der Waals Potential : An Important Complement to Molecular Electrostatic Potential in Studying Intermolecular Interactions Van Der Waals Potential : An Important Complement to Molecular Electrostatic Potential in Studying Intermolecular Interactions. **2020**, https://doi.org/10.26434/chemrxiv.12148572.v1.
67. Boto, R.A.; Philip, J.; García, J.C. Revealing Strong Interactions with the Reduced Density Gradient : A Benchmark for Covalent, Ionic and Charge - Shift Bonds. *Theor. Chem. Acc.* **2017**, 1–9, https://doi.org/10.1007/s00214-017-2169-9.
68. Ross, R.T.D.Á.N.L. The Electron Localization Function : A Tool for Locating Favorable Proton Docking Sites in the Silica Polymorphs. **2003**, 305–316, https://doi.org/10.1007/s00269-003-0318-2.
69. Lu, T.; Chen, Q. A Simple Method of Identifying π Orbitals for Non - Planar Systems and a Protocol of Studying π Electronic Structure. *Theor. Chem. Acc.* **2020**, *2*, https://doi.org/10.1007/s00214-019-2541-z.
70. Tsirelson, V. Research Papers Analyzing Experimental Electron Density with the Localized-Orbital Locator Research Papers. **2002**, 780–785, https://doi.org/10.1107/S0108768102012338.
71. Fuster, F.; Sevin, A.; Silvi, B. Topological Analysis of the Electron Localization Function (ELF) Applied to the Electrophilic Aromatic Substitution. *Acs Publication* **2000**, *2*, 852–858, https://doi.org/10.1021/jp992783k.
72. Rahuman, M.H.; Muthu, S.; Raajaraman, B.R.; Raja, M. Quantum Computational, Spectroscopic and Molecular Docking Studies on 2-Acetylthiophene and Its Bromination Derivative. *J. Mol. Struct.* **2020**, *1212*, 128129, https://doi.org/10.1016/j.molstruc.2020.128129.
73. Campo, J.M.; G, L. The Reduced Density Gradient in Atoms. *Int. J. Quantum Chemistry* **2012**, *128369*, 1–5, https://doi.org/10.1002/qua.24241.
74. Silva, P. De; Corminboeuf, C. Covalent Interactions Using Regions of Density Overlap Simultaneous Visualization of Covalent and Noncovalent Interactions Using Regions of Density Overlap. *Acs Publication* **2014**, https://doi.org/10.1021/ct500490b.
75. Schmider, H.L.; Becke, A.D. Chemical Content of the Kinetic Energy Density Q. Journal of Molecular Structure Theochem **2000**, *527*, http://dx.doi.org/10.1016/S0166-1280(00)00477-2.
76. Jacobsen, H. Localized-Orbital Locator (LOL) Profiles of Chemical. **2008**, *702*, 695–702, http://dx.doi.org/10.1139/V08-052.
77. Liu, Z.; Lu, T.; Chen, Q. An Sp-Hybridized All-Carboatomic Ring, Cyclo [18] Carbon : Electronic Structure, Electronic Spectrum, and Optical Nonlinearity. *Carbon N. Y.* **2020**, *165*, 461–467, http://dx.doi.org/10.1016/j.carbon.2020.05.023.
78. Prabakaran, A.; Vijayakumar, V.; Chidambaram, R.; Muthu, S. Computational Analysis of Novel N, N - Dimethyl-. *Polycycl. Aromat. Compd.* **2020**, *0*, 1–17, http://dx.doi.org/10.1080/10406638.2020.1756356.
79. Sevvanthi, S.; Muthu, S.; Raja, M.; Aayisha, S.; Janani, S. Heliyon PES, Molecular Structure, Spectroscopic (FT-IR, FT-Raman), Electronic (UV-Vis, HOMO-LUMO), Quantum Chemical and Biological (Docking) Studies on a Potent Membrane Permeable Inhibitor : Dibenzoxepine Derivative. *Heliyon* **2020**, *6*, e04724, https://doi.org/10.1016/j.heliyon.2020.e04724.
80. Nagar, P.R.; Gajjar, N.D.; Dhameliya, T.M. In Search of SARS CoV-2 Replication Inhibitors: Virtual Screening, Molecular Dynamics Simulations and ADMET Analysis. *J. Mol. Struct.* **2021**, *1246*, 131190, https://doi.org/10.1016/j.molstruc.2021.131190.
81. Wadapurkar, R.M.; Shilpa, M.D.; Katti, A.K.S.; Sulochana, M.B. In Silico Drug Design for Staphylococcus Aureus and Development of Host-Pathogen Interaction Network. *Informatics Med. Unlocked* **2018**, *10*, 58–70, https://doi.org/10.1016/j.imu.2017.11.002.
82. Davella, R.; Gurrapu, S.; Mamidala, E. Phenolic Compounds as Promising Drug Candidates against COVID-19 - an Integrated Molecular Docking and Dynamics Simulation Study. *Mater. Today Proc.* **2021**, 1–6, https://doi.org/10.1016/j.matpr.2021.05.595.
83. Elangovan, N.; Thomas, R.; Sowrirajan, S. Synthesis of Schiff Base (E) -4- ((2-Hydroxy-3, 5-Diiodobenzylidene) Amino) -N-Thiazole-2-Yl) Benzenesulfonamide with Antimicrobial Potential, Structural Features, Experimental Biological Screening and Quantum Mechanical Studies. *J. Mol. Struct.* **2022**, *1250*, 131762, https://doi.org/10.1016/j.molstruc.2021.131762.
84. Elangovan, N.; Sowrirajan, S.; Manoj, K.P.; Kumar, A.M. Synthesis, Structural Investigation, Computational Study, Antimicrobial Activity and Molecular Docking Studies of Novel Synthesized (E)-4-((Pyridine-4-Ylmethylene)Amino)-N-(Pyrimidin-2-Yl)Benzenesulfonamide from Pyridine-4-Carboxaldehyde and Sulfadiazine. *J. Mol. Struct.* **2021**, *1241*, https://doi.org/10.1016/j.molstruc.2021.130544.
85. Oyebamiji, A.K.; Josiah, O.M.; Akintelu, S.A.; Adeoye, M.D.; Sabitu, B.O.; Latona, D.F.; Esan, A.O.; Soetan, E.A.; Semire, B. Dataset on Insightful Bio-Evaluation of 2-(Quinoline-4-Yloxy)Acetamide Analogues as Potential Anti-Mycobacterium Tuberculosis Catalase-Peroxidase Agents via in Silico Mechanisms. *Data Br.* **2021**, *38*, 107441, https://doi.org/10.1016/j.dib.2021.107441.
86. Ali, H.I.; Tomita, K.; Akaho, E.; Kambara, H.; Miura, S.; Hayakawa, H.; Ashida, N.; Kawashima, Y.;

Yamagishi, T.; Ikeya, H.; et al. Antitumor Studies. Part 1: Design, Synthesis, Antitumor Activity, and AutoDock Study of 2-Deoxo-2-Phenyl-5-Deazaflavins and 2-Deoxo-2-Phenylflavin-5-Oxides as a New Class of Antitumor Agents. *Bioorganic Med. Chem.* **2007**, *15*, 242–256, https://doi.org/10.1016/j.bmc.2006.09.063.

87. Elghoneimy, L.K.; Ismail, M.I.; Boeckler, F.M.; Azzazy, H.M.E.; Ibrahim, T.M. Facilitating SARS CoV-2 RNA-Dependent RNA Polymerase (RdRp) Drug Discovery by the Aid of HCV NS5B Palm Subdomain Binders: In Silico Approaches and Benchmarking. *Comput. Biol. Med.* **2021**, *134*, 104468, https://doi.org/10.1016/j.compbiomed.2021.104468.
88. Sriramulu, D.K.; Wu, S.; Lee, S.G. Effect of Ligand Torsion Number on the AutoDock Mediated Prediction of Protein-Ligand Binding Affinity. *J. Ind. Eng. Chem.* **2020**, *83*, 359–365, https://doi.org/10.1016/j.jiec.2019.12.009.

Supplementary materials

Table S1. Optimized parameters of compound C2.

Bond	Length
(C1,C2)	1.5221
(C1,C14)	1.5314
(C1,H30)	1.0962
(C1,H31)	1.0919
(C2,C3)	1.5173
(C2,C6)	1.5428
(C2,H32)	1.0997
(C3,O4)	1.2076
(C3,C10)	1.5098
(C5,C6)	1.5261
(C5,C15)	1.5244
(C5,H33)	1.097
(C5,H34)	1.0946
(C6,C7)	1.5371
(C6,H35)	1.0998
(C7,C8)	1.5287
(C7,C9)	1.5376
(C7,H36)	1.0982
(C8,C11)	1.5244
(C8,H37)	1.0925
(C8,H38)	1.0955
(C9,C10)	1.5425
(C9,C13)	1.5429
(C9,H39)	1.0944
(C10,H40)	1.0894
(C10,H41)	1.0939
(C11,C12)	1.5333
(C11,H42)	1.0978
(C11,H43)	1.0937
(C12,C13)	1.5467
(C12,C16)	1.5278
(C12,H44)	1.0981
(C13,C17)	1.5416
(C13,H45)	1.0978
(C14,C15)	1.5266
(C14,C27)	1.5388
(C14,H46)	1.0989
(C15,O28)	1.4239
(C15,H47)	1.1016
(C16,H48)	1.0927
(C16,H49)	1.0938
(C16,H50)	1.0881
(C17,C18)	1.5465
(C17,O19)	1.4242
(C17,H51)	1.0994
(C18,C20)	1.5514
(C18,C21)	1.5302
(C18,H52)	1.0929
(O19,H53)	0.9594
(C20,C22)	1.5229
(C20,C23)	1.5312
(C20,H54)	1.098
(C21,H55)	1.0925
(C21,H56)	1.0906
(C21,H57)	1.089
(C22,O24)	1.4186
(C22,H58)	1.0983
(C22,H59)	1.0963
(C23,H60)	1.0921

Bond	Length
(C23,H61)	1.0943
(C23,H62)	1.0913
(O24,C26)	1.3923
(O25,C26)	1.4015
(O25,H63)	0.9604
(C26,H64)	1.0932
(C26,H65)	1.0956
(C27,N29)	1.4557
(C27,H66)	1.0964
(C27,H67)	1.0942
(O28,H68)	0.9591
(N29,H69)	1.0135
(N29,H70)	1.0133
(C2,C1,C14)	113.0355
(C2,C1,H30)	108.8826
(C2,C1,H31)	109.6377
(C14,C1,H30)	109.6439
(C14,C1,H31)	109.6691
(H30,C1,H31)	105.7077
(C1,C2,C3)	112.8571
(C1,C2,C6)	111.3511
(C1,C2,H32)	109.0594
(C3,C2,C6)	109.66
(C3,C2,H32)	106.1441
(C6,C2,H32)	107.497
(C2,C3,O4)	122.8863
(C2,C3,C10)	114.8512
(O4,C3,C10)	122.2369
(C6,C5,C15)	112.0039
(C6,C5,H33)	109.6332
(C6,C5,H34)	110.5504
(C15,C5,H33)	109.6657
(C15,C5,H34)	107.7847
(H33,C5,H34)	107.0648
(C2,C6,C5)	109.2965
(C2,C6,C7)	113.3754
(C2,C6,H35)	106.332
(C5,C6,C7)	113.665
(C5,C6,H35)	107.3274
(C7,C6,H35)	106.362
(C6,C7,C8)	114.9893
(C6,C7,C9)	109.9122
(C6,C7,H36)	106.678
(C8,C7,C9)	111.2501
(C8,C7,H36)	106.7874
(C9,C7,H36)	106.7448
(C7,C8,C11)	110.9321
(C7,C8,H37)	110.1069
(C7,C8,H38)	110.6977
(C11,C8,H37)	109.3838
(C11,C8,H38)	109.4307
(H37,C8,H38)	106.1696
(C7,C9,C10)	110.5651
(C7,C9,C13)	111.6914
(C7,C9,H39)	105.9694
(C10,C9,C13)	113.605
(C10,C9,H39)	106.7839
(C13,C9,H39)	107.7697
(C3,C10,C9)	110.1983
(C3,C10,H40)	108.2131
(C3,C10,H41)	108.0686
(C9,C10,H40)	112.248

Bond	Length
(C9,C10,H41)	110.3272
(H40,C10,H41)	107.6505
(C8,C11,C12)	113.9809
(C8,C11,H42)	109.172
(C8,C11,H43)	109.689
(C12,C11,H42)	108.1801
(C12,C11,H43)	109.2323
(H42,C11,H43)	106.2935
(C11,C12,C13)	109.4664
(C11,C12,C16)	109.077
(C11,C12,H44)	107.8697
(C13,C12,C16)	115.3164
(C13,C12,H44)	107.7187
(C16,C12,H44)	107.1266
(C9,C13,C12)	109.9972
(C9,C13,C17)	113.1841
(C9,C13,H45)	106.7845
(C12,C13,C17)	113.6166
(C12,C13,H45)	106.9431
(C17,C13,H45)	105.7983
(C1,C14,C15)	109.3367
(C1,C14,C27)	110.0592
(C1,C14,H46)	108.8836
(C15,C14,C27)	112.8494
(C15,C14,H46)	107.4272
(C27,C14,H46)	108.1758
(C5,C15,C14)	111.5763
(C5,C15,O28)	110.7457
(C5,C15,H47)	108.9675
(C14,C15,O28)	108.7474
(C14,C15,H47)	107.6039
(O28,C15,H47)	109.1206
(C12,C16,H48)	110.9981
(C12,C16,H49)	109.4798
(C12,C16,H50)	112.3852
(H48,C16,H49)	108.2428
(H48,C16,H50)	107.2217
(H49,C16,H50)	108.3826
(C13,C17,C18)	115.9793
(C13,C17,O19)	106.1664
(C13,C17,H51)	107.5711
(C18,C17,O19)	109.6953
(C18,C17,H51)	108.462
(O19,C17,H51)	108.7604
(C17,C18,C20)	110.0121
(C17,C18,C21)	110.6049
(C17,C18,H52)	108.4884
(C20,C18,C21)	115.3273
(C20,C18,H52)	104.7907
(C21,C18,H52)	107.2278
(C17,O19,H53)	108.8523
(C18,C20,C22)	114.163
(C18,C20,C23)	110.3219
(C18,C20,H54)	109.9103
(C22,C20,C23)	108.6829
(C22,C20,H54)	105.283
(C23,C20,H54)	108.2211
(C18,C21,H55)	110.3337
(C18,C21,H56)	110.9349
(C18,C21,H57)	111.7248
(H55,C21,H56)	107.5387
(H55,C21,H57)	107.8039

Bond	Length
(H56,C21,H57)	108.3525
(C20,C22,O24)	109.5422
(C20,C22,H58)	109.7397
(C20,C22,H59)	110.7578
(O24,C22,H58)	108.611
(O24,C22,H59)	110.5068
(H58,C22,H59)	107.6359
(C20,C23,H60)	111.2633
(C20,C23,H61)	110.5334
(C20,C23,H62)	111.9533
(H60,C23,H61)	108.0523
(H60,C23,H62)	107.4766
(H61,C23,H62)	107.378
(C22,O24,C26)	113.7814
(C26,O25,H63)	108.0926
(O24,26,O25)	113.217
(O24,C26,H64)	105.6177
(O24,C26,H65)	111.1734
(O25,C26,H64)	111.4947
(O25,C26,H65)	105.3901
(H64,C26,H65)	110.0291
(C14,C27,29)	117.5334
(C14,C27,H66)	108.4764
(C14,C27,H67)	108.3672
(N29,C27,H66)	108.2655
(N29,C27,H67)	107.734
(H66,C27,C67)	105.8706
(C15,O28,C68)	108.6693
(C27,N29,H69)	109.9954
(C27,N29,H70)	109.2752
(H69,N29,H70)	106.5085
(C14,C1,C2,C3)	-179.3184
(C14,C1,C2,C6)	-55.484
(C14,C1,C2,H32)	62.9789
(H30,C1,C2,C3)	-57.2105
(H30,C1,C2,C6)	66.624
(H30,C1,C2,H32)	-174.9132
(H31,C1,C2,C3)	57.9937
(H31,C1,C2,C6)	-178.1719
(H31,C1,C2,H32)	-59.709
(C2,C1,C14,C15)	54.7439
(C2,C1,C14,C27)	179.2319
(C2,C1,C14,H46)	-62.3523
(H30,C1,C14,C15)	-66.9365
(H30,C1,C14,C27)	57.5515
(H30,C1,C14,H46)	175.9673
(H31,C1,C14,C15)	177.4143
(H31,C1,C14,C27)	-58.0977
(H31,C1,C14,H46)	60.3181
(C1,C2,C3,O4)	-1.2629
(C1,C2,C3,C10)	176.9326
(C6,C2,C3,O4)	-126.0245
(C6,C2,C3,C10)	52.1709
(H32,C2,C3,O4)	118.1398
(H32,C2,C3,C10)	-63.6647
(C1,C2,C6,C5)	54.7003
(C1,C2,C6,C7)	-177.3739
(C1,C2,C6,H35)	-60.8577
(C3,C2,C6,C5)	-179.6708
(C3,C2,C6,C7)	-51.745
(C3,C2,C6,H35)	64.7712
(H32,C2,C6,C5)	-64.6963

Bond	Length
(H32,C2,C6,C7)	63.2294
(H32,C2,C6,H35)	179.7457
(C2,C3,C10,C9)	-55.5344
(C2,C3,C10,H40)	-178.6105
(C2,C3,C10,H41)	65.0873
(O4,C3,C10,C9)	122.6741
(O4,C3,C10,H40)	-0.402
(O4,C3,C10,H41)	-116.7043
(C15,C5,C6,C2)	-56.409
(C15,C5,C6,C7)	175.8275
(C15,C5,C6,H35)	58.5102
(H33,C5,C6,C2)	-178.3831
(H33,C5,C6,C7)	53.8534
(H33,C5,C6,H35)	-63.4639
(H34,C5,C6,C2)	63.811
(H34,C5,C6,C7)	-63.9525
(H34,C5,C6,H35)	178.7303
(C6,C5,C15,C14)	58.0612
(C6,C5,C15,O28)	179.3508
(C6,C5,C15,H47)	-60.6119
(H33,C5,C15,C14)	-179.9834
(H33,C5,C15,O28)	-58.6937
(O33,C5,C15,H47)	61.3436
(H34,C5,C15,C14)	-63.7578
(H34,C5,C15,O28)	57.5319
(H34,C5,C15,H47)	177.5692
(2,C6,C7,C8)	-71.0032
(C2,C6,C7,C9)	55.4476
(C2,C6,C7,H36)	170.8144
(C5,C6,C7,C8)	54.6218
(C5,C6,C7,C9)	-178.9275
(C5,C6,C7,H36)	-63.5607
(H35,C6,C7,C8)	172.4982
(H35,C6,C7,C9)	-61.051
(H35,C6,C7,C36)	54.3157
(C6,C7,C8,C11)	178.6327
(C6,C7,C8,H37)	-60.1398
(C6,C7,C8,H38)	56.9465
(C9,C7,C8,C11)	52.8708
(C9,C7,C8,H37)	174.0983
(C9,C7,C8,H38)	-68.8154
(H36,C7,C8,C11)	-63.2463
(H36,C7,C8,H37)	57.9813
(H36,C7,C8,H38)	175.0676
(C6,C7,C9,C10)	-57.053
(C6,C7,C9,C13)	175.3927
(C6,C7,C9,H39)	58.2979
(C8,C7,C9,C10)	71.4794
(C8,C7,C9,C13)	-56.0749
(C8,C7,C9,H39)	-173.1697
(H36,C7,C9,C10)	-172.3774
(H36,C7,C9,H13)	60.0683
(H36,C7,C9,H39)	-57.0265
(C7,C8,C11,C12)	-54.0332
(C7,C8,C11,C42)	67.0443
(C7,C8,C11,H43)	-176.8587
(H37,C8,C11,C12)	-175.6853
(H37,C8,C11,H42)	-54.6078
(H37,C8,C11,H43)	61.4893
(H38,C8,C11,C12)	68.392
(H38,C8,C11,H42)	-170.5305
(H38,C8,C11,H43)	-54.4335

Bond	Length
(C7,C9,C10,C3)	56.8271
(C7,C9,C10,H40)	177.5118
(C7,C9,C10,H41)	-62.4289
(C13,C9,C10,C3)	-176.6772
(C13,C9,C10,H40)	-55.9925
(C13,C9,C10,H41)	64.0668
(H39,C9,C10,C3)	-58.0127
(H39,C9,C10,H40)	62.672
(H39,C9,C10,H41)	-177.2688
(C7,C9,C13,C12)	57.7522
(C7,C9,C13,C17)	-173.9591
(C7,C9,C13,H45)	-57.9494
(C10,C9,C13,C12)	-68.1487
(C10,C9,C13,C17)	60.14
(C10,C9,C13,H45)	176.1497
(H39,C9,C13,C12)	173.7543
(H39,C9,C13,C17)	-57.957
(H39,C9,C13,H45)	58.0528
(C8,C11,C12,C13)	55.5943
(C8,C11,C12,C16)	-177.3826
(C8,C11,C12,H44)	-61.3495
(H42,C11,C12,C13)	-66.0334
(H42,C11,C12,C16)	60.9897
(H42,C11,C12,H44)	177.0227
(H43,C11,C12,C13)	178.6688
(H43,C11,C12,C16)	-54.3081
(H43,C11,C12,H44)	61.725
(C11,C12,C13,C9)	-56.0999
(C11,C12,C13,C17)	175.8495
(C11,C12,C13,H45)	59.5016
(C16,C12,C13,C9)	-179.5142
(C16,C12,C13,C17)	52.4353
(C16,C12,C13,H45)	-63.9127
(H44,C12,C13,C9)	60.9391
(H44,C12,C13,C17)	-67.1115
(H44,C12,C13,H45)	176.5406
(C11,C12,C16,H48)	-68.1829
(C11,C12,C16,H49)	51.2523
(C11,C12,C16,H50)	171.7469
(C13,C12,C16,H48)	55.4369
(C13,C12,C16,H49)	174.8721
(C13,C12,C16,H50)	-64.6333
(H44,C12,C16,H48)	175.3094
(H44,C12,C16,H49)	-65.2554
(H44,C12,C16,H50)	55.2391
(C9,C13,C17,C18)	38.3054
(C9,C13,C17,O19)	160.4187
(C9,C13,C17,H51)	-83.2834
(C12,C13,C17,C18)	164.6953
(C12,C13,C17,O19)	-73.1914
(C12,C13,C17,H51)	43.1066
(H45,C13,C17,C18)	-78.2876
(H45,C13,C17,O19)	43.8258
(H45,C13,C17,H51)	160.1237
(C1,C14,C15,C5)	-55.2318
(C1,C14,C15,O28)	-177.6755
(C1,C14,C15,H47)	64.2515
(C27,C14,C15,C5)	-178.0733
(C27,C14,C15,O28)	59.483
(C27,C14,C15,H47)	-58.59
(H46,C14,C15,C5)	62.7797
(H46,C14,C15,O28)	-59.664

Bond	Length
(H46,C14,C15,H47)	-177.737
(C1,C14,C27,N29)	162.2262
(C1,C14,C27,H66)	-74.6227
(C1,C14,C27,H67)	39.8805
(C15,C14,C27,N29)	-75.3363
(C15,C14,C27,H66)	47.8148
(C15,C14,C27,H67)	162.318
(H46,C14,C27,N29)	43.3759
(H46,C14,C27,H66)	166.527
(H46,C14,C27,H67)	-78.9698
(C5,C15,O28,C68)	58.998
(C14,C15,O28,C68)	-178.0574
(H47,C15,O28,C68)	-60.9478
(C13,C17,C18,C20)	-164.9521
(C13,C17,C18,C21)	66.4885
(C13,C17,C18,H52)	-50.8565
(O19,C17,C18,C20)	74.8227
(O19,C17,C18,C21)	-53.7366
(O19,C17,C18,H52)	-171.0816
(H51,C17,C18,C20)	-43.839
(H51,C17,C18,C21)	-172.3983
(C51,C17,C18,H52)	70.2567
(C13,C17,O19,H53)	-178.9114
(C18,C17,O19,H53)	-52.8828
(H51,C17,O19,H53)	65.5944
(C17,C18,C20,C22)	-159.5683
(C17,C18,C20,C23)	77.7108
(C17,C18,C20,H54)	-41.5494
(C21,C18,C20,C22)	-33.6424
(C21,C18,C20,C23)	-156.3634
(C21,C18,C20,H54)	84.3765
(H52,C18,C20,C22)	83.9941
(H52,C18,C20,C23)	-38.7268
(H52,C18,C20,H54)	-157.987
(C17,C18,C21,H55)	-54.6059
(C17,C18,C21,H56)	-173.6748
(C17,C18,C21,H57)	65.306
(C20,C18,C21,H55)	179.7726
(C20,C18,C21,H56)	60.7038
(C20,C18,C21,H57)	-60.3154
(H52,C18,C21,H55)	63.5116
(H52,C18,C21,H56)	-55.5573
(H52,C18,C21,H57)	-176.5764
(C18,C20,C22,O24)	80.3115
(C18,C20,C22,H58)	-160.5346
(C18,C20,C22,H59)	-41.834
(C23,C20,C22,H24)	-156.0793
(C23,C20,C22,H58)	-36.9254
(C23,C20,C22,H59)	81.7752
(H54,C20,C22,O24)	-40.3209
(H54,C20,C22,H58)	78.8331
(H54,C20,C22,H59)	-162.4664
(C18,C20,C23,H60)	-172.7942
(C18,C20,C23,H61)	67.1505
(C18,C20,C23,H62)	-52.509
(C22,C20,C23,H60)	61.3311
(C22,C20,C23,H61)	-58.7243
(C22,C20,C23,H62)	-178.3838
(H54,C20,C23,H60)	-52.5133
(H54,C20,C23,H61)	-172.5686
(H54,C20,C23,H62)	67.7718
(C20,C22,O24,C26)	-171.9022

Bond	Length
(H58,C22,O24,C26)	68.2501
(H59,C22,O24,C26)	-49.6067
(C22,O24,C26,O25)	71.0759
(C22,O24,C26,H64)	-166.6551
(C22,O24,C26,H65)	-47.3375
(H63,O25,C26,O24)	64.0574
(H63,O25,C26,H64)	-54.8738
(H63,O25,C26,H65)	-174.2266
(C14,C27,N29,H69)	-65.7955
(C14,C27,N29,H70)	50.794
(H66,C27,N29,H69)	170.9464
(H66,C27,N29,H70)	-72.4641
(H67,C27,N29,H69)	56.874
(H67,C27,N29,H70)	173.4634

Table S2. Frontier molecular orbital properties of the compound C2.

Property	Values
εHOMO	-9.9
εLUMO	-4.9
Energy gap ΔE	5.0
Ionisation energy (*I*= εHOMO= -HOMO)	9.9
Electron Affinity (*A*= εLUMO= -LUMO)	4.9
Global hardness (Ƞ = (*I*-*A*)/2)	2.5
Global softness (*S =1/Ƞ)*	0.4
Chemical Potential (μ = -(I+*A*)/2)	-7.4
Electronegativity (χ = -μ)	7.4
Electrophilicity index (ω = μ2/2Ƞ)	8.3
Nucleophilicity index (*N* = 1/ω)	0.1
Electronaccepting power (ω+ = *A*2/2(*I*-*A*)	0.5
Electrondonating power (ω+ = *I*2/2(*I*-*A*)	0.9

Table S3. Natural population analysis of the compound C2.

	Natural	Natural Population			
Atom No	Charge	Core	Valance	Rydberg	Total
C 1	-0.47452	1.99917	4.46163	0.01371	6.47452
C 2	-0.342	1.99899	4.33255	0.01046	6.342
C 3	0.57247	1.99913	3.39319	0.03521	5.42753
O 4	-0.53265	1.99977	6.52894	0.00394	8.53265
C 5	-0.49394	1.99912	4.48376	0.01106	6.49394
C 6	-0.24733	1.99908	4.2365	0.01176	6.24733
C 7	-0.25098	1.99907	4.23998	0.01193	6.25098
C 8	-0.47327	1.99917	4.46482	0.00928	6.47327
C 9	-0.25072	1.99909	4.24057	0.01106	6.25072
C 10	-0.5577	1.99908	4.5482	0.01043	6.5577
C 11	-0.46482	1.99918	4.45594	0.00969	6.46482
C 12	-0.24917	1.9991	4.23998	0.01009	6.24917
C 13	-0.26928	1.99904	4.256	0.01424	6.26928
C 14	-0.29444	1.99903	4.28373	0.01168	6.29444
C 15	0.08716	1.99891	3.90059	0.01333	5.91284
C 16	-0.68881	1.99928	4.6832	0.00633	6.68881
C 17	0.09035	1.99895	3.89583	0.01487	5.90965
C 18	-0.2816	1.99907	4.27226	0.01027	6.2816
O 19	-0.7641	1.9998	6.75815	0.00615	8.7641
C 20	-0.2706	1.99908	4.25975	0.01177	6.2706
C 21	-0.69918	1.99928	4.69186	0.00803	6.69918
C 22	-0.13736	1.99906	4.12705	0.01125	6.13736
C 23	-0.70238	1.99928	4.69718	0.00592	6.70238
O 24	-0.59716	1.99979	6.59093	0.00644	8.59716
O 25	-0.76008	1.99981	6.75443	0.00584	8.76008
C 26	0.15759	1.99934	3.82619	0.01688	5.84241
C 27	-0.27576	1.99919	4.26153	0.01504	6.27576
O 28	-0.76989	1.99979	6.76414	0.00596	8.76989
N 29	-0.91534	1.99954	5.90548	0.01032	7.91534

	Natural	Natural Population			
Atom No	Charge	Core	Valance	Rydberg	Total
H 30	0.24712	0.0000	0.75042	0.00246	0.75288
H 31	0.26403	0.0000	0.73409	0.00189	0.73597
H 32	0.26258	0.0000	0.73517	0.00225	0.73742
H 33	0.24003	0.0000	0.75778	0.00219	0.75997
H 34	0.24728	0.0000	0.75007	0.00265	0.75272
H 35	0.24788	0.0000	0.74938	0.00273	0.75212
H 36	0.25391	0.0000	0.74372	0.00237	0.74609
H 37	0.24849	0.0000	0.75005	0.00146	0.75151
H 38	0.22879	0.0000	0.76944	0.00177	0.77121
H 39	0.25256	0.0000	0.74531	0.00213	0.74744
H 40	0.26231	0.0000	0.73502	0.00267	0.73769
H 41	0.25762	0.0000	0.74092	0.00146	0.74238
H 42	0.23425	0.0000	0.76349	0.00225	0.76575
H 43	0.24769	0.0000	0.75069	0.00162	0.75231
H 44	0.23123	0.0000	0.76628	0.00249	0.76877
H 45	0.2614	0.0000	0.7357	0.00291	0.7386
H 46	0.24462	0.0000	0.75184	0.00353	0.75538
H 47	0.21776	0.0000	0.77908	0.00316	0.78224
H 48	0.24092	0.0000	0.7576	0.00148	0.75908
H 49	0.22683	0.0000	0.77168	0.00149	0.77317
H 50	0.25175	0.0000	0.74689	0.00136	0.74825
H 51	0.21785	0.0000	0.77979	0.00236	0.78215
H 52	0.24508	0.0000	0.75221	0.00271	0.75492
H 53	0.47552	0.0000	0.52293	0.00156	0.52448
H 54	0.23436	0.0000	0.76145	0.00419	0.76564
H 55	0.23183	0.0000	0.76691	0.00126	0.76817
H 56	0.23454	0.0000	0.76326	0.00219	0.76546
H 57	0.25339	0.0000	0.74417	0.00244	0.74661
H 58	0.21968	0.0000	0.77789	0.00243	0.78032
H 59	0.23128	0.0000	0.76564	0.00307	0.76872
H 60	0.24464	0.0000	0.75418	0.00118	0.75536
H 61	0.24343	0.0000	0.75512	0.00145	0.75657
H 62	0.23883	0.0000	0.76017	0.001	0.76117
H 63	0.47756	0.0000	0.52013	0.00231	0.52244
H 64	0.21396	0.0000	0.78397	0.00206	0.78604
H 65	0.20793	0.0000	0.78916	0.00292	0.79207
H 66	0.2268	0.0000	0.77078	0.00242	0.7732
H 67	0.23569	0.0000	0.76269	0.00162	0.76431
H 68	0.47389	0.0000	0.524	0.00212	0.52611
H 69	0.37511	0.0000	0.62304	0.00185	0.62489
H 70	0.40509	0.0000	0.59271	0.00221	0.59491

Table S4. Second-order petribution theory fock matrix analysis of compound C2.

Donar	Type	ED/e	Acceptor	Type	ED/e	E(2)[a]	E(j-i)[b]	F(i,j)[c]
C 1 - C 2	σ	1.97778	C 1 - C 14	σ*	0.01734	0.8	0.97	0.025
			C 1 - H 30	σ*	0.01583	0.6	1.03	0.022
			C 1 - H 31	σ*	0.01119	0.77	1.05	0.025
			C 2 - C 3	σ*	0.06274	1.03	0.98	0.029
			C 2 - C 6	σ*	0.03064	1.31	0.93	0.031
			C 2 - H 32	σ*	0.02178	0.94	1.01	0.028
			C 3 - C 10	σ*	0.05269	2.26	0.98	0.042
			C 6 - C 7	σ*	0.02409	2.21	0.95	0.041
			C 14 - C 27	σ*	0.04038	1.77	0.96	0.037
C 1 - C 14	σ	1.97123	C 1 - C 2	σ*	0.0175	0.95	0.96	0.027
			C 14 - C 15	σ*	0.03099	0.71	0.94	0.023
			C 14 - C 27	σ*	0.04038	0.62	0.95	0.022
			C 14 - H 46	σ*	0.02227	0.66	1.02	0.023
			C 15 - O 28	σ*	0.02878	3.21	0.8	0.045
			C 27 - N 29	σ*	0.00733	2.34	0.96	0.042
C 1 - H 30	σ	1.98063	C 2 - H 32	σ*	0.02178	2.92	0.9	0.046
			C 14 - H 46	σ*	0.02227	2.66	0.92	0.044
C 1 - H 31	σ	1.97972	C 1 - C 2	σ*	0.0175	0.56	0.86	0.02
C 2 - C 3	σ	1.97959	C 1 - C 2	σ*	0.0175	1.06	1.01	0.029
			C 10 - H 40	σ*	0.01169	1.14	1.09	0.032
C 2 - C 6	σ	1.95801	C 1 - C 2	σ*	0.0175	1.03	0.96	0.028
			C 3 - O 4	π*	0.01345	2.75	0.58	0.036

Donar	Type	ED/e	Acceptor	Type	ED/e	E(2)[a]	E(j-i)[b]	F(i,j)[c]
			C 5 - C 6	σ*	0.02071	0.72	0.94	0.023
			C 5 - H 33	σ*	0.01228	1.69	1	0.037
			C 6 - H 35	σ*	0.02032	0.5	1	0.02
			C 7 - H 36	σ*	0.0181	1.24	1.01	0.032
C 2 - H 32	σ	1.95484	C 1 - H 30	σ*	0.01583	2.56	0.94	0.044
			C 3 - O 4	π*	0.01345	5.7	0.49	0.048
			C 6 - H 35	σ*	0.02032	2.52	0.92	0.043
C 3 - O 4	σ	1.9959	C 2 - C 3	σ*	0.06274	0.81	1.45	0.031
			C 3 - C 10	σ*	0.05269	0.74	1.45	0.03
C 3 - O 4	π	1.98343	C 2 - C 6	σ*	0.03024	1.54	0.7	0.03
			C 2 - H 32	σ*	0.02178	1.8	0.78	0.034
			C 9 - C 10	σ*	0.02531	1.63	0.7	0.03
			C 10 - H 41	σ*	0.01537	1.86	0.79	0.034
C 3 - C 10	σ	1.98417	C 1 - C 2	σ*	0.0175	1.92	1.02	0.039
			C 2 - C 3	σ*	0.06274	0.53	1.02	0.021
			C 9 - C 10	σ*	0.02531	1.12	0.97	0.03
			C 9 - C 13	σ*	0.02323	2.24	0.99	0.042
			C 10 - H 40	σ*	0.01169	0.8	1.09	0.026
			C 10 - H 41	σ*	0.01537	0.79	1.06	0.026
C 5 - C 6	σ	1.97308	C 5 - C 15	σ*	0.02695	0.76	0.96	0.024
			C 5 - H 33	σ*	0.01228	0.73	1.02	0.024
			C 5 - H 34	σ*	0.01614	0.72	1.03	0.024
			C 6 - C 7	σ*	0.02409	1	0.96	0.028
			C 6 - H 35	σ*	0.02032	0.76	1.01	0.025
			C 7 - C 9	σ*	0.02528	1.82	0.95	0.037
			C 15 - O 28	σ*	0.02878	2.75	0.82	0.042
C 5 - C 15	σ	1.98275	C 14 - C 27	σ*	0.04038	2.08	0.98	0.041
			C 15 - H 47	σ*	0.03098	0.51	1.03	0.021
C 5 - H 33	σ	1.9798	C 14 - C 15	σ*	0.03099	3.09	0.87	0.046
C 5 - H 34	σ	1.97969	C 15 - O 28	σ*	0.02878	0.59	0.72	0.018
			C 15 - H 47	σ*	0.03098	2.66	0.92	0.044
C 6 - C 7	σ	1.97304	C 7 - H 36	σ*	0.0181	0.79	1.02	0.025
			C 8 - C 11	σ*	0.01254	1.56	0.97	0.035
			C 9 - C 13	σ*	0.02323	2.14	0.95	0.04
C 6 - H 35	σ	1.97261	C 2 - H 32	σ*	0.02178	2.69	0.91	0.044
			C 5 - H 34	σ*	0.01614	2.8	0.92	0.046
C 7 - C 8	σ	1.97855	C 8 - H 37	σ*	0.01076	0.77	1.03	0.025
			C 8 - H 38	σ*	0.01566	0.62	1.02	0.022
			C 9 - H 39	σ*	0.01792	1.42	1.02	0.034
			C 11 - H 43	σ*	0.01046	1.47	1.03	0.035
C 7 - C 9	σ	1.97148	C 7 - H 36	σ*	0.0181	0.72	1.01	0.024
			C 8 - H 37	σ*	0.01076	1.61	1.03	0.036
			C 9 - C 10	σ*	0.02531	0.75	0.92	0.023
			C 9 - C 13	σ*	0.02323	1.15	0.94	0.029
			C 9 - H 39	σ*	0.01792	0.81	1.02	0.026
C 7 - H 36	σ	1.96989	C 8 - H 38	σ*	0.01566	2.98	0.92	0.047
C 8 - C 11	σ	1.98315	C 11 - C 12	σ*	0.01961	0.8	0.95	0.025
			C 11 - H 42	σ*	0.01565	0.56	1.02	0.021
			C 11 - H 43	σ*	0.01046	0.66	1.03	0.023
C 8 - H 37	σ	1.98067	C 11 - C 12	σ*	0.01961	3.38	0.86	0.048
C 8 - H 38	σ	1.98103	C 11 - H 42	σ*	0.01565	2.55	0.93	0.043
C 9 - C 10	σ	1.96467	C 10 - H 41	σ*	0.01537	0.85	1.01	0.026
			C 13 - H 45	σ*	0.01995	1.16	1.02	0.031
C 9 - C 13	σ	1.96919	C 13 - H 45	σ*	0.01995	0.61	1.02	0.022
			C 17 - O 19	σ*	0.02557	1.87	0.81	0.035
C 9 - H 39	σ	1.97318	C 10 - H 41	σ*	0.01537	2.71	0.92	0.045
			C 12 - C 13	σ*	0.02784	3.04	0.85	0.045
C 10 - H 40	σ	1.98071	C 9 - C 10	σ*	0.02531	0.77	0.84	0.023
			C 10 - H 41	σ*	0.01537	0.51	0.93	0.019
C 10 - H 41	σ	1.96404	C 3 - O 4	π*	0.01345	1.57	1.03	0.036
			C 9 - H 39	σ*	0.01792	2.33	0.95	0.042
C 11 - C 12	σ	1.9778	C 12 - H 44	σ*	0.02126	0.66	1.01	0.023
			C 13 - C 17	σ*	0.02732	2.64	0.93	0.044
			C 16 - H 50	σ*	0.00718	1.59	1.05	0.037
C 11 - H 42	σ	1.98171	C 8 - H 38	σ*	0.01566	2.72	0.92	0.045
			C 12 - H 44	σ*	0.02126	2.7	0.92	0.045
C 11 - H 43	σ	1.98192	C 7 - C 8	σ*	0.02422	3.26	0.85	0.047
			C 12 - C 13	σ*	0.02784	3.2	0.84	0.046
C 12 - C 13	σ	1.97307	C 12 - H 44	σ*	0.02126	0.59	1.01	0.022
			C 13 - C 17	σ*	0.02732	0.9	0.93	0.026

Donar	Type	ED/e	Acceptor	Type	ED/e	E(2)[a]	E(j-i)[b]	F(i,j)[c]
			C 13 - H 45	σ*	0.01995	0.85	1.01	0.026
			C 16 - H 49	σ*	0.00785	1.19	1.02	0.031
C 12 - C 16	σ	1.9828	C 12 - H 44	σ*	0.02126	0.74	1.01	0.024
			C 16 - H 48	σ*	0.00814	0.58	1.03	0.022
			C 16 - H 49	σ*	0.00785	0.53	1.02	0.021
			C 16 - H 50	σ*	0.00718	0.75	1.05	0.025
C 12 - H 44	σ	1.97246	C 16 - H 48	σ*	0.00814	2.62	0.94	0.044
C 13 - C 17	σ	1.97503	C 17 - H 51	σ*	0.02842	0.75	1.03	0.025
			C 18 - C 20	σ*	0.02904	1.45	0.94	0.033
			O 19 - H 53	σ*	0.00953	1.69	1.01	0.037
C 13 - H 45	σ	1.96839	C 17 - H 51	σ*	0.02842	2.26	0.91	0.041
C 14 - C 15	σ	1.97298	C 15 - H 47	σ*	0.03098	0.63	1.02	0.023
			C 27 - H 67	σ*	0.01206	1.02	1.05	0.029
			O 28 - H 68	σ*	0.00782	1.73	1	0.037
C 14 - C 27	σ	1.98054	C 14 - C 15	σ*	0.03099	0.89	0.94	0.026
			C 14 - H 46	σ*	0.02227	0.78	1.01	0.025
			C 27 - H 67	σ*	0.01206	0.52	1.03	0.021
C 14 - H 46	σ	1.97122	C 27 - H 66	σ*	0.02101	2.17	0.93	0.04
C 15 - O 28	σ	1.99217	C 1 - C 14	σ*	0.01734	1.58	1.16	0.038
C 15 - H 47	σ	1.98025	C 5 - H 34	σ*	0.01614	2.57	0.94	0.044
			C 14 - H 46	σ*	0.02227	2.68	0.95	0.045
C 16 - H 48	σ	1.99015	C 12 - H 44	σ*	0.02126	2.53	0.91	0.043
C 16 - H 49	σ	1.98864	C 12 - C 13	σ*	0.02784	3.83	0.83	0.051
C 16 - H 50	σ	1.98947	C 11 - C 12	σ*	0.01961	2.71	0.84	0.043
			C 12 - C 16	σ*	0.01198	0.52	0.86	0.019
C 17 - C 18	σ	1.97813	C 18 - H 52	σ*	0.01985	0.83	1.03	0.026
			C 20 - C 22	σ*	0.01957	1.97	0.96	0.039
			C 21 - H 56	σ*	0.00841	1.56	1.05	0.036
C 17 - O 19	σ	1.99199	C 9 - C 13	σ*	0.02323	1.88	1.13	0.041
			C 18 - H 52	σ*	0.01985	1.2	1.22	0.034
C 17 - H 51	σ	1.98075	C 13 - H 45	σ*	0.01995	2.17	0.95	0.04
			C 18 - C 21	σ*	0.01453	2.87	0.88	0.045
C 18 - C 20	σ	1.97423	C 21 - H 55	σ*	0.00714	1.31	1.03	0.033
			C 22 - H 58	σ*	0.02106	1.16	1.01	0.031
			C 23 - H 60	σ*	0.00549	1.38	1.02	0.034
C 18 - C 21	σ	1.98348	C 21 - H 55	σ*	0.00714	0.67	1.03	0.024
			C 21 - H 56	σ*	0.00841	0.69	1.04	0.024
			C 21 - H 57	σ*	0.00939	0.66	1.05	0.024
C 18 - H 52	σ	1.9703	C 17 - O 19	σ*	0.02557	3.94	0.72	0.048
			C 21 - H 57	σ*	0.00939	2.59	0.95	0.045
O 19 - H 53	σ	1.98968	C 13 - C 17	σ*	0.02732	2.03	1.07	0.042
C 20 - C 22	σ	1.98008	C 23 - H 62	σ*	0.00712	1.68	1.05	0.038
			O 24 - C 26	σ*	0.05687	1.97	0.86	0.037
C 20 - C 23	σ	1.98013	C 23 - H 61	σ*	0.00795	0.5	1.02	0.02
			C 23 - H 62	σ*	0.00712	0.63	1.03	0.023
C 20 - H 54	σ	1.97015	C 22 - H 59	σ*	0.02253	2.4	0.93	0.042
			C 23 - H 61	σ*	0.00795	2.63	0.93	0.044
C 21 - H 55	σ	1.98763	C 18 - C 20	σ*	0.02904	3.62	0.83	0.049
			C 18 - C 21	σ*	0.01453	0.54	0.86	0.019
C 21 - H 56	σ	1.98841	C 17 - C 18	σ*	0.03515	3.01	0.84	0.045
C 21 - H 57	σ	1.99014	C 18 - C 21	σ*	0.01453	0.52	0.85	0.019
			C 18 - H 52	σ*	0.01985	2.47	0.93	0.043
C 22 - O 24	σ	1.98995	C 20 - C 23	σ*	0.01093	1.42	1.12	0.036
			C 26 - H 64	σ*	0.02339	0.94	1.21	0.03
C 22 - H 58	σ	1.98833	C 18 - C 20	σ*	0.02904	3.08	0.86	0.046
			C 20 - C 22	σ*	0.01957	0.58	0.88	0.02
C 22 - H 59	σ	1.98835	C 20 - H 54	σ*	0.02431	2.17	0.95	0.041
C 23 - H 60	σ	1.98977	C 18 - C 20	σ*	0.02904	3.07	0.85	0.046
C 23 - H 61	σ	1.98996	C 20 - H 54	σ*	0.02431	2.52	0.93	0.043
C 23 - H 62	σ	1.98834	C 17 - H 51	σ*	0.02842	0.57	0.94	0.021
			C 20 - C 22	σ*	0.01957	2.59	0.87	0.043
O 24 - C 26	σ	1.99243	C 20 - C 22	σ*	0.01957	1.25	1.17	0.034
O 25 - H 63	σ	1.99151	C 26 - H 65	σ*	0.02792	1.76	1.16	0.04
C 26 - H 64	σ	1.98812	C 22 - O 24	σ*	0.02524	3.6	0.78	0.047
C 26 - H 65	σ	1.98818	O 25 - H 63	σ*	0.00998	3.01	0.94	0.048
C 27 - N 29	σ	1.99455	C 1 - C 14	σ*	0.01734	1.34	1.06	0.034
C 27 - H 66	σ	1.98211	C 14 - H 46	σ*	0.02227	2.68	0.92	0.044
			N 29 - H 69	σ*	0.00713	2.91	0.97	0.048
C 27 - H 67	σ	1.98312	C 14 - C 15	σ*	0.03099	3.25	0.85	0.047
			N 29 - H 70	σ*	0.01578	2.99	1	0.049

Donar	Type	ED/e	Acceptor	Type	ED/e	E(2)[a]	E(j-i)[b]	F(i,j)[c]
O 28 - H 68	σ	1.99133	C 14 - C 15	σ*	0.03099	2.25	1.08	0.044
N 29 - H 69	σ	1.99182	C 27 - H 66	σ*	0.02101	2.08	1.04	0.042
N 29 - H 70	σ	1.99179	C 27 - H 67	σ*	0.01206	2.14	1.05	0.042
LP(1)	O 4	1.97672	C 2 - C 3	σ*	0.06274	1.91	1.07	0.041
LP(2)	O 4	1.90407	C 2 - C 3	σ*	0.06274	19.03	0.65	0.1
LP(2)	O 4	1.90407	C 3 - C 10	σ*	0.05269	17.98	0.65	0.097
LP(1)	O 19	1.97954	C 17 - H 51	σ*	0.02842	1.47	1.01	0.034
LP(2)	O 19	1.96184	C 17 - C 18	σ*	0.03515	5.46	0.64	0.053
LP(2)	O 19	1.96184	C 17 - H 51	σ*	0.02842	4	0.73	0.048
LP(1)	O 24	1.96978	C 26 - H 65	σ*	0.02792	1.93	1.01	0.039
LP(2)	O 24	1.9077	O 25 - C 26	σ*	0.05372	14.75	0.52	0.079
LP(1)	O 25	1.9847	C 26 - H 64	σ*	0.02339	1.98	1.03	0.04
LP(2)	O 25	1.93118	O 24 - C 26	σ*	0.05687	14.04	0.56	0.079
LP(1)	O 28	1.97805	C 15 - H 47	σ*	0.03098	2.81	0.97	0.047
LP(2)	O 28	1.98327	C 5 - C 15	σ*	0.02695	5.94	0.71	0.058
LP(1)	N 29	1.95112	C 14 - C 27	σ*	0.04038	9.91	0.6	0.069
LP(1)	N 29	1.95112	C 27 - H 66	σ*	0.02101	2.65	0.68	0.038